Electronic supplementary information for :

Above Room Temperature Spin Crossover in Mononuclear Iron(II) Complexes Featuring Pyridyl-Benzimidazole Bidentate Ligands Adorned with Aliphatic Chains

Alexandra Šagátová,[a] Kamil Kotrle,[b] Barbora Brachňaková,[a] Lubomír Havlíček,[cd] Ivan Nemec,[bc] Radovan Herchel,[b] Monika Hofbauerova,[e] Yuriy Halahovets,[e] Peter Šiffalovič,[e] Erik Čižmár,[f] Ondřej F. Fellner,[b] Ivan Šalitroš*[ac]

[a)] Department of Inorganic Chemistry, Faculty of Chemical and Food Technology, Slovak University of Technology in Bratislava. Bratislava SK-81237, Slovakia. *e-mail: ivan.salitros@stuba.sk
[b)] Department of Inorganic Chemistry, Faculty of Science, Palacký University, 17. listopadu 12, 771 46 Olomouc, Czech Republic
[c)] Central European Institute of Technology, Brno University of Technology, Purkyňova 123, 61200 Brno Czech Republic
[d)] Institute of Physics of Materials, Czech Academy of Sciences, Žižkova 22, 61662 Brno, Czech Republic
[e)] Institute of Physics, Slovak Academy of Sciences, 84511 Bratislava, Slovakia; Centre of Excellence for Advanced Materials Application, 84511 Bratislava.
[f)] Institute of Physics, Faculty of Science, P.J. Šafárik University, Park Angelinum 9, 04154 Košice, Slovakia.

S1 Experimental part

S1.1 Synthesis

Materials and methods:

All purchased compounds ($Fe(ClO_4)_2.6H_2O$, $Fe(BF_4)_2.6H_2O$, $Fe(CF_3SO_3)_2$, K_2CO_3, 1-bromopentane, 1-bromoheptane) and solvents (acetonitrile p.a., methanol p.a., acetone p.a., nitromethane p. a., diethyl ether p.a., diisopropyl ether p.a., tert-butyl-methyl ether p.a., N,N-dimethylformamid) were used as received without any further purification. 2-pyridin-2-yl-1*H*-benzimidazole was prepared according reported synthetic procedure.[1] IR spectra in the interval from 4000 to 400 cm^{-1} of herein reported compounds were measured on Nicolet 5700 spectrometer (ATR technique). Elemental analysis of carbon, hydrogen and nitrogen was carried out by EA CHNS(O) Flash 1112 machine The UV-VIS spectra were measured in solid state on Specord 200 spectrophotometer in the range of 800 – 200 nm.

Synthesis of 1-pentyl-2-(pyridin-2-yl)-1*H*-benzimidazole (**L1**)

2-pyridin-2-yl-1*H*-benzimidazole (3 g, 15.27 mmol) was dissolved in DMF (5 mL), followed by the addition of K_2CO_3 (2.23 g, 15.41 mmol, 1.05 eq.) to the stirred solution at 80 °C. After 1 hour of stirring, 1-bromopentane (2.79 g, 18.44 mmol, 1.20 eq.) was added dropwise, and the reaction was further stirred at 80 °C for an additional 24 hours. After completion of the reaction, the mixture was cooled to room temperature, and the residual DMF was removed by vacuum distillation. The crude reaction mixture was then subjected to three consecutive extractions with a chloroform/water mixture (3:1). The organic extracts were combined, and the chloroform was evaporated using a rotary evaporator. Purification was achieved through column chromatography using an eluent mixture of ethyl acetate/chloroform with a ratio of 1:9. The resulting desired product, 1-pentyl-2-(pyridin-2-yl)-1H-benzimidazole (2.45 g, 9.22 mmol), was obtained as orange-yellow oil in 60% yield. **^{1}H NMR** (400 MHz, $CDCl_3$, δ ppm) 8.61 (ddd, *J* = 4.8, 1.9, 0.9 Hz, 1H), 8.36 (dt, *J* = 8.0, 1.1 Hz, 1H), 7.81 (m, 1 H), 7.76 (m, 1 H), 7.39 (m, 1 H), 7.25 (m, 3 H), 4.75 (m, 2H), 1.81 (m, 2H), 1.27 (m, 4H), 0.87 (m, 3H); **^{13}C NMR** (101 MHz, $CDCl_3$ δ ppm) 148.62; 136.70; 124.65; 123.65; 123.20; 122.47; 120.10; 110.25; 45.44 (C-H_2); 29.76 (C-H_2); 28.98 (C-H_2); 22.25 (C-H_2); 13.96 (C-H_3). **FT-IR** (ATR / cm^{-1}): 3050 (w), ν(Car-H), 2953 (m), 2927 (m), 2857 (m) ν(Cal-H), 1589 (m), 1566 (m), 1509 (w), 1464 (m), 1434 (s), 1330 (m) ν(C_{ar}-C_{ar}, C_{ar}-N), 793 (m), 734 (s), 699 (m) δ(C_{ar}-H). **UV-VIS** (EtOH, λ / nm) 240 ($\pi\rightarrow\pi^*$), 306 ($n\rightarrow\pi^*$).

Synthesis of 1-heptyl-2-(pyridin-2-yl)-1*H*-benzimidazole (**L2**)

2-pyridin-2-yl-1*H*-benzimidazole (3 g, 15.27 mmol) was dissolved in DMF (5 mL), followed by the addition of K_2CO_3 (2.23 g, 15.41 mmol, 1.05 eq.) to the stirred solution at 80 °C. After 1 hour of stirring, 1-bromopentane (2.76 g, 18.32 mmol, 1.20 eq.) was added dropwise, and the reaction was further stirred at 80 °C for an additional 24 hours. After completion of the reaction, the mixture was cooled to RT, and the residual DMF was removed by vacuum distillation. The crude reaction mixture was then subjected to three consecutive extractions with a chloroform/water mixture. The organic extracts were combined, and the chloroform was evaporated using a rotary evaporator. Purification was achieved through column chromatography using an eluent mixture of ethyl acetate/chloroform with a ratio of 1:9. The resulting desired product, 1-heptyl-2-(pyridin-2-yl)-1H-benzimidazole (2.39 g, 8.15 mmol), was obtained as orange-yellow oil in 53% yield. **^{1}H NMR** (400 MHz, $CDCl_3$, δ ppm) 8.69 (ddd, *J* = 4.9, 1.8, 0.9 Hz, 1H), 8.40 (dt, *J* = 7.9, 1.1 Hz, 1H), 7.84 (m, 2H), 7.45 (m, 1H), 7.32 (m, 3H). 4.82 (t, 2H), 1.87 (m, 2H), 1.27 (m, 8 H), 0.86 (t, *J* = 6.9 Hz, 3H). **^{13}C NMR** (101 MHz, $CDCl_3$, δ ppm): 148.74; 136.82; 124.81; 123.78; 123.30; 122.57; 120.22; 110.36; 45.57 (C-H_2); 31.81 (C-H_2); 30.17 (C-H_2); 28.96 (C-H_2); 26.91 (C-H_2); 22.71 (C-H_2); 14.19 (C-H_3). FT-IR (ATR / cm^{-1}): 3050.7 (w) ν(Car-H), 2954 (w), 2923 (m), 2953 (m) ν(Cal-H), 1590 (m), 1566 (m), 1509 (w), 1464 (m), 1435 (s), 1330 (m) ν(C_{ar}-C_{ar}, C_{ar}-N), 792 (m), 737 (s), 699 (m) δ(Car-H). **UV-VIS** (EtOH, λ / nm): 239 ($\pi\rightarrow\pi^*$), 305 ($n\rightarrow\pi^*$).

Preparation of coordination compounds **1**–**5**

All procedures were done in 15 mL solvent under an inert atmosphere at RT. The solution of ligand was bubbled with nitrogen gas for 20 minutes, one equivalent of appropriate ferrous salt was added which was accompanied by immediate colour change from orange to violet and reaction mixture was further stirred at RT another two hours. The suitable crystals for the single-crystal X-ray diffraction analysis were obtained by a diffuse crystallisation of fresh solutions in either *tert*-butyl methyl ether or diethyl ether atmosphere. The compounds were characterized by elemental analysis, FT-IR (Figure S3) and UV-VIS spectroscopy (Figure S4).

Compound **1** - **$[Fe(L1)_3](ClO_4)_2$**
The $Fe(ClO_4)_2.6H_2O$ (50.1 mg, 0.138 mmol, 1.1 eq) was added into the nitromethane solution of **L1** (100 mg, 0.377 mmol, 3 eq.), reaction mixture was stirred for three hours at RT, filtered, and left for crystallisation by slow diffusion of diethyl ether atmosphere at 5°C. After several days, the dark single crystals were collected in a 46 % yield (54.9mg, 0.0578 mmol). **Elemental analysis** for $C_{51}H_{57}Cl_2O_8FeN_9$ (M_w=1050.80 g/mol, $[Fe(L1)_3](ClO_4)_2$): C 58.11% (58.29%), H 5.30%, (5.47%); N 11.59% (12.00%). **FT-IR** (ATR / cm^{-1}): 3078 (w) $\nu(C_{ar}\text{-}H)$, 2927 (w), 2862 (w) $\nu(C_{al}\text{-}H)$, 1601 (w), 1544 (w), 1509 (w), 1484 (w), 1437 (m) $\nu(C_{ar}\text{-}C_{ar}, C_{ar}\text{-}N)$, 744 (s), 621 (s) $\delta(C_{ar}\text{-}H)$. **UV-VIS** (EtOH, λ / nm): 345 ($\pi\rightarrow\pi^*$), 415 ($n\rightarrow\pi^*$), 547 (MLCT); **UV-VIS** (nujol, λ / nm): 335 ($\pi\rightarrow\pi^*$), 397 ($n\rightarrow\pi^*$), 533 (MLCT).

Compound **2** - **$[Fe(L1)_3](BF_4)_2.(C_2H_5)_2O$**
The $Fe(BF_4)_2.6H_2O$ (45.3 mg, 0.134 mmol, 1.1 eq.) was added into the nitromethane solution of **L1** (97 mg, 0.366 mmol, 3 eq.), reaction mixture was stirred for three hours at RT, filtered, and left for crystallisation by slow diffusion of diethyl ether atmosphere at 5°C. After several days, the dark single crystals were collected in a 22 % yield (29.5 mg, 0.0268 mmol). **Elemental analysis** for $C_{51}H_{57}B_2F_8FeN_9$ (M_w=1025.51 g/mol, $[Fe(L1)_3](BF_4)_2$): C 58.99% (59.73%), H 5.12% (5.60%), N 11.89% (12.29%). **FT-IR** (ATR / cm^{-1}): 3080 (w) $\nu(C_{ar}\text{-}H)$, 2929 (w), 2859 (w) $\nu(C_{al}\text{-}H)$, 1602 (w), 1548 (w), 1511 (w), 1484 (w), 1461 (w), 1439 (m) $\nu(C_{ar}\text{-}C_{ar}, C_{ar}\text{-}N)$, 741 (s) $\delta(C_{ar}\text{-}H)$. **UV-VIS** (EtOH, λ / nm): 337 ($\pi\rightarrow\pi^*$), 412 ($n\rightarrow\pi^*$) 557 (MLCT); **UV-VIS** (nujol, λ / nm): 328 ($\pi\rightarrow\pi^*$), 392 ($n\rightarrow\pi^*$) 528 (MLCT).

Compound **3** - **$[Fe(L1)_3](CF_3SO_3)_2$**
The $Fe(CF_3SO_3)_2$ (50.4 mg, 0.142 mmol, 1.1 eq) was added into the acetone solution of **L1** (103 mg, 0.388 mmol, 3 eq), reaction mixture was stirred for three hours at RT, filtered, and left for crystallisation by slow diffusion of *tert*-butylmethyl ether atmosphere at 5°C. After several days, the dark single crystals were collected in a 27 % yield (40.1 mg, 0.0349 mmol). **Elemental analysis** for $C_{59}H_{69}F_6FeN_9O_6S_2$ (M_w=1234.20 g/mol, $[Fe(L1)_3](CF_3SO_3)_2$): C 56.75% (57.42%), H 5.02% (5.64%), N 9.81% (10.21%). **FT-IR** (ATR / cm^{-1}): 3129 (w), 3072 (w) $\nu(C_{ar}\text{-}H)$, 2928 (w), 2857 (w) $\nu(C_{al}\text{-}H)$, 1604 (w), 1511 (w), 1483 (w), 1458 (w), 1439 (m) $\nu(C_{ar}\text{-}C_{ar}, C_{ar}\text{-}N)$, 745 (s), 634 (s) $\delta(C_{ar}\text{-}H)$; **UV-VIS** (nujol, λ / nm): 336 ($\pi\rightarrow\pi^*$), 407 ($n\rightarrow\pi^*$), 545 (MLCT); **UV-VIS** (nujol, λ / nm): 319 ($\pi\rightarrow\pi^*$), 389 ($n\rightarrow\pi^*$), 518 (MLCT).

Compound **4** - **$[Fe(L2)_3](ClO_4)_2$**
The $Fe(ClO_4)_2.6H_2O$ (46.3 mg, 0.128 mmol, 1.1 eq) was added into the acetonitrile solution of **L2** (102 mg, 0.348 mmol, 3 eq.), reaction mixture was stirred for three hours at RT, filtered, and left for crystallisation by slow diffusion of diethyl ether atmosphere atmosphere at 5°C. After several days, the dark single crystals were collected in a 34 % yield (48.9 mg, 0.0429 mmol). **Elemental analysis** for $C_{57}H_{69}Cl_2O_8FeN_9$ (M_w=1134.96 g/mol, $[Fe(L2)_3](ClO_4)_2$): C 58.89% (60.32%), H 5.51% (6.13%), N 10.57% (11.11%). **FT-IR** (ATR / cm^{-1}): 3127 (w), 3070 (w) $\nu(C_{ar}\text{-}H)$, 2924 (w), 2852 (w) $\nu(C_{al}\text{-}H)$, 1602 (w), 1510 (w), 1483 (w), 1456 (w), 1439 (m) $\nu(C_{ar}\text{-}C_{ar}, C_{ar}\text{-}N)$, 741 (s), 620 (s) $\delta(C_{ar}\text{-}H)$. **UV-VIS** (EtOH, λ / nm): 335 ($\pi\rightarrow\pi^*$), 396 ($n\rightarrow\pi^*$), 550 (MLCT); **UV-VIS** (nujol, λ / nm): 320 ($\pi\rightarrow\pi^*$), 392 ($n\rightarrow\pi^*$), 531 (MLCT);

Compound **5** - **$[Fe(L2)_3](BF_4)_2.CH_3NO_2$**
The $Fe(BF_4)_2.6H_2O$ (39.7 mg, 0.118 mmol, 1.1 eq) was added into the nitromethane solution of **L2** (94 mg, 0.320 mmol, 3 eq), reaction mixture was stirred for three hours at RT, filtered, and left for crystallisation by slow diffusion of diethyl ether atmosphere atmosphere at 5°C. After several days, the dark single crystals were collected in a 19 % yield (23.8 mg, 0.0203 mmol). **Elemental analysis** for $C_{58}H_{72}B_2F_8FeN_{10}O_2$ (M_w=1170.71 g/mol, $[Fe(L2)_3](BF_4)_2$): C 58.99% (59.50%), H 5.12% (6.20%), N 10.85% (11.96%). **FT-IR** (ATR / cm^{-1}): 3133 (w), 3080 (w) $\nu(C_{ar}\text{-}H)$ 2925 (w), 2854 (w) $\nu(C_{al}\text{-}H)$, 1602 (w), 1552 (w), 1509 (w), 1485 (w), 1463 (w), 1439 (m) $\nu(C_{ar}\text{-}C_{ar}, C_{ar}\text{-}N)$, 746 (s) $\delta(C_{ar}\text{-}H)$. **UV-VIS** (EtOH, λ / nm): 331 ($\pi\rightarrow\pi^*$), 399 ($n\rightarrow\pi^*$), 538 (MLCT); **UV-VIS** (nujol, λ / nm): 324 ($\pi\rightarrow\pi^*$), 387 ($n\rightarrow\pi^*$), 508 and 549 (MLCT).

S1.2 Single-crystal diffraction analysis

The single-crystal diffraction data for reported compounds were collected using an XtaLAB Synergy-I diffractometer with a HyPix3000 hybrid pixel array detector and microfocused PhotonJet-I X-ray source (Cu Kα). The absorption corrections were applied using the program CrysAlisPro 1.171.40.82a.[2] The structure was solved using SHELXT[3] program and refined by the full matrix least-squares procedure with SHELX[4] in OLEX2 (version 1.5).[5] All non-hydrogen atoms were refined anisotropically. All hydrogen atoms were found from the Fourier difference map and refined using the "riding" model. Non-routine aspects of crystal structure refinement:

1: the collected diffraction data were of poor quality because the crystal quality was significantly affected by rapid solvent loss. This led to weak diffracting power and also lower agreement among the intensities of equivalent diffractions (R_{int} > 8%). Consequently, the model quality is low, and *R*-factor is considerably larger than the value standardly accepted by IUCr (R_1 below 8%). We attempted to address the issues arising from solvent loss, such as the disorder of perchlorate anions and aliphatic chains, by establishing positional disorders in the model. However, we failed to significantly improve the model, and R1 only showed slight improvement. Additionally, we employed a solvent masking procedure[6] to subtract the electron density corresponding to two nitromethane molecules per asymmetric unit.

2: The positional disorders of the BF_4^- anions were modelled as disorder over two positions, together with disorder of the aliphatic chain.

3: The positional disorders of the $CF_3SO_3^-$ anions and one of the aliphatic chains were modelled as disorder over two positions.

4: The disorder of the aliphatic chain was modelled as disorder over two positions.

S1.3 Magnetic measurements

All herein reported magnetic measurements were performed on a MPMS-3 or PPMS EverCool II magnetometers (Quantum Design). The temperature dependent magnetization was recorded at B_{DC} = 0.1 T as an external magnetic field. The temperature sweeping rate was 1 K min^{-1} the same for cooling and for heating modes. Each temperature data point was stabilized for 1 minutes before the measurement. Gelatine capsule (standard measurements in the dark) was used as sample holders in the temperature range 1.8 ↔ 400 K. The very small diamagnetic contribution of the gelatine capsule was negligible to the overall magnetization, which was dominated by sample. The diamagnetic corrections of the molar magnetic susceptibilities were applied using Pascal constants.[7]

S1.4 Computational studies

All theoretical calculations were performed with use of ORCA 5.0.3. program package.[8] Initial structures, obtained from X-ray were treated by DFT hydrogen optimization, with BP86 functional[9], with basis sets from Ahlrich def2 basis set[10], TZVPP basis for Fe and TZVP for other atoms, and def2/J auxiliary basis. CASSCF calculations were done with TZVPP basis for Fe and TZVP basis for all other

atoms, and with def2/J and def2-TZVP/C auxiliary basis sets. Dynamic correlation was treated by RI-NEVPT2 method[11]. CASSCF was performed for 6 electrons in 5 *d*-orbitals (selected by ORCA keyword "actorbs dorbs"), which responds to Fe(II) valence electron sphere. Number of calculated roots responds to maximal number of possible roots, 5 state with multiplicity M_S = 5, 45 roots with M_S = 3 and 50 roots with M_S =1. CASSCF calculations were done with "NoFrozenCore" keyword. Crystal field parameters were obtained with help of Ab Initio Ligand Field Theory (AILFT) module.[12]All calculations were performed with help of RIJCOSX approximation[13], with improved integral precision, enabled by "DEFGRID3" ORCA keyword, and strict convergence "TightSCF" settings. For visualization, software Avogadro[14] and Mercury[15] was used. Tanabe-Sugano diagrams were created with help of web application.[16] ChatGPT[17] was used for correction of grammar and stylistics in certain parts of the text.

S1.5 Self-assembly of SCO molecular layers

Typical experimental conditions for SCO layer formation involved silanization of silicon surface by dip coating a hydrophilic silicon wafer (1x1 cm; UV-ozone treated) in a 1 mM OTS (octadecyltrichlorosilane) solution in toluene overnight at room temperature to prepare an OTS self-assembled monolayer (SAM). The excess amount of physisorbed OTS was removed by sonication of OTS SAM wafer in toluene. Organosilane SAMs provide desirable surface properties such as improved wettability and chemical affinity to transfer a monolayer interfacial film onto the silicon wafer. In the next step, OTS-SAM/silicon wafer was placed inside a Petri dish with a slight horizontal tilt before the SCO Iron (II) complex was distributed onto the cyclohexane subphase. 80 µL of the SCO Iron (II) complex with a concentration of 1mg/mL in methanol was gently spread on the surface of cyclohexane (9 x 1.5 cm2; volume 4 mL) in a Petri dish by a microsyringe. The self-assembly process on the OTS/silicon wafer took place after the complete evaporation of cyclohexane.

S2 Spectral characterisation of reported compounds

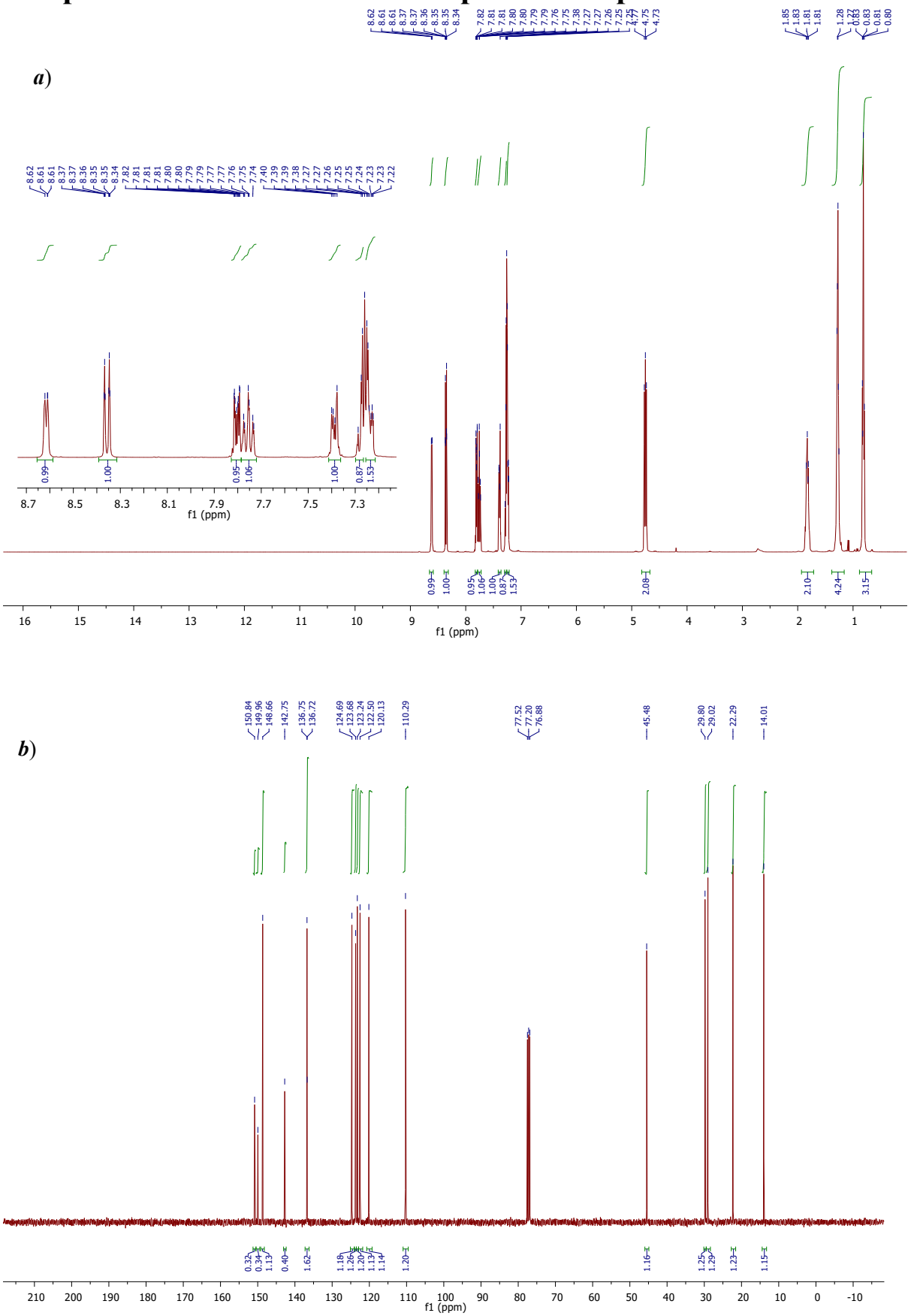

Figure S1. **a**) ^{1}H-NMR and **b**) ^{13}C-NMR spectra of ligand **L1**

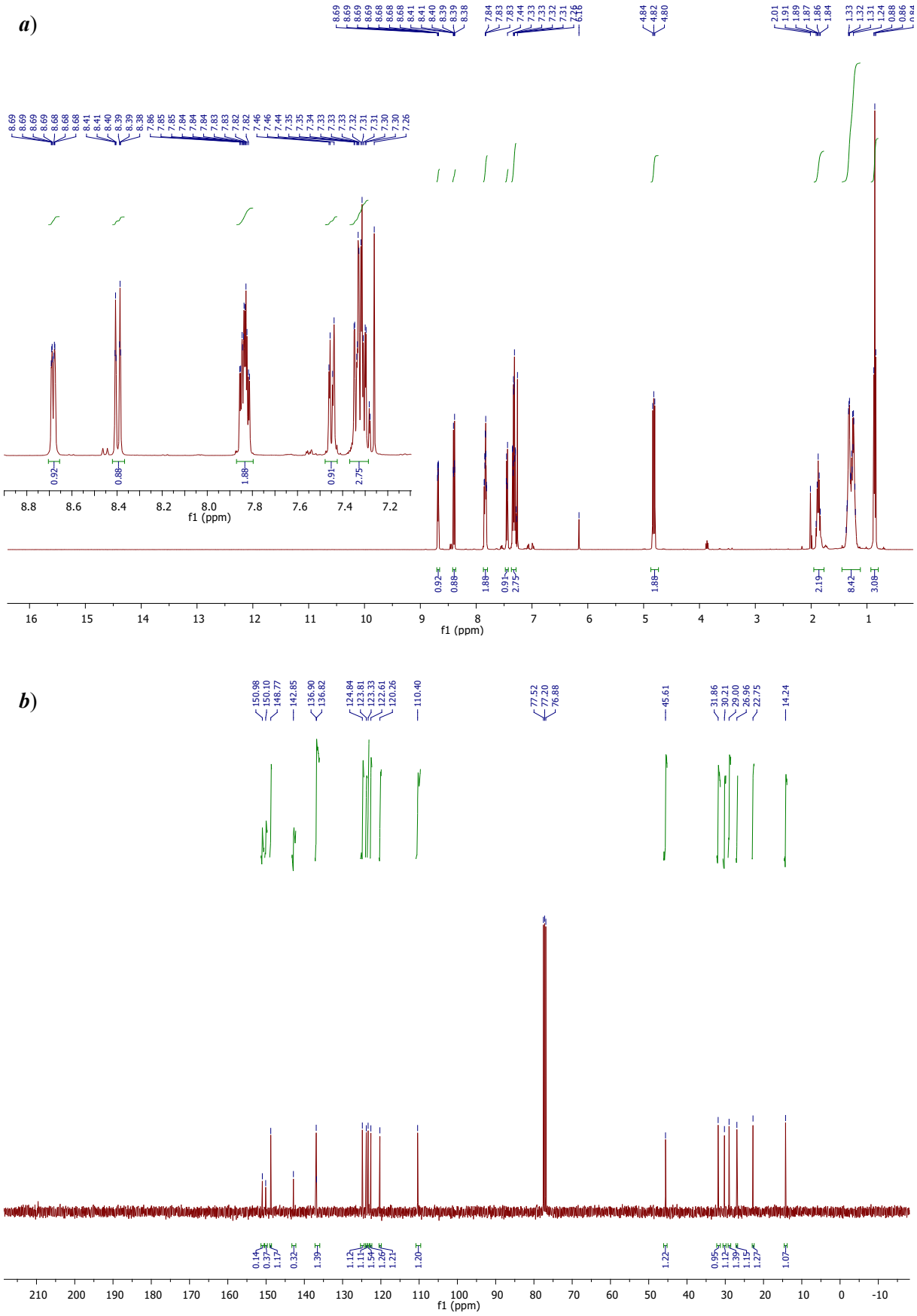

Figure S2. a) ^{1}H-NMR and **b**) ^{13}C-NMR spectra of ligand **L2**

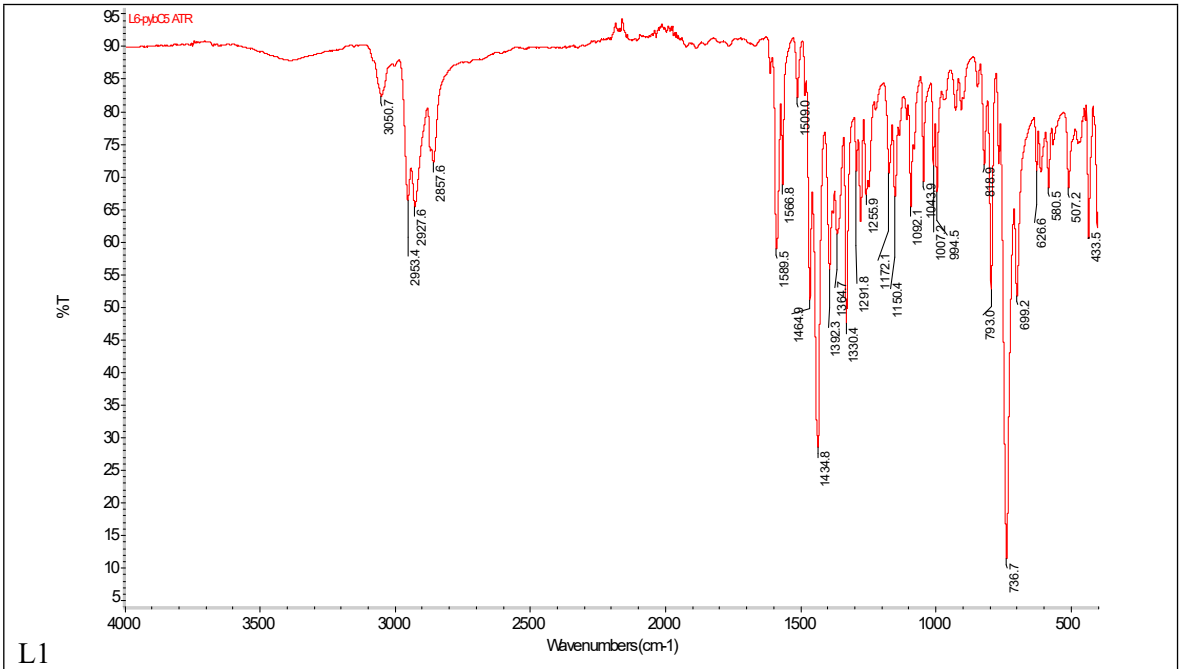
L6-pybC5 ATR
%T
Wavenumbers(cm-1)
3050.7
2953.4
2927.6
2857.6
1589.5
1566.8
1509.0
1464.9
1434.8
1392.3
1364.7
1330.4
1291.8
1255.9
1172.1
1150.4
1092.7
1043.9
1007.2
994.5
818.8
793.0
736.7
699.2
626.6
580.5
507.2
433.5

L1

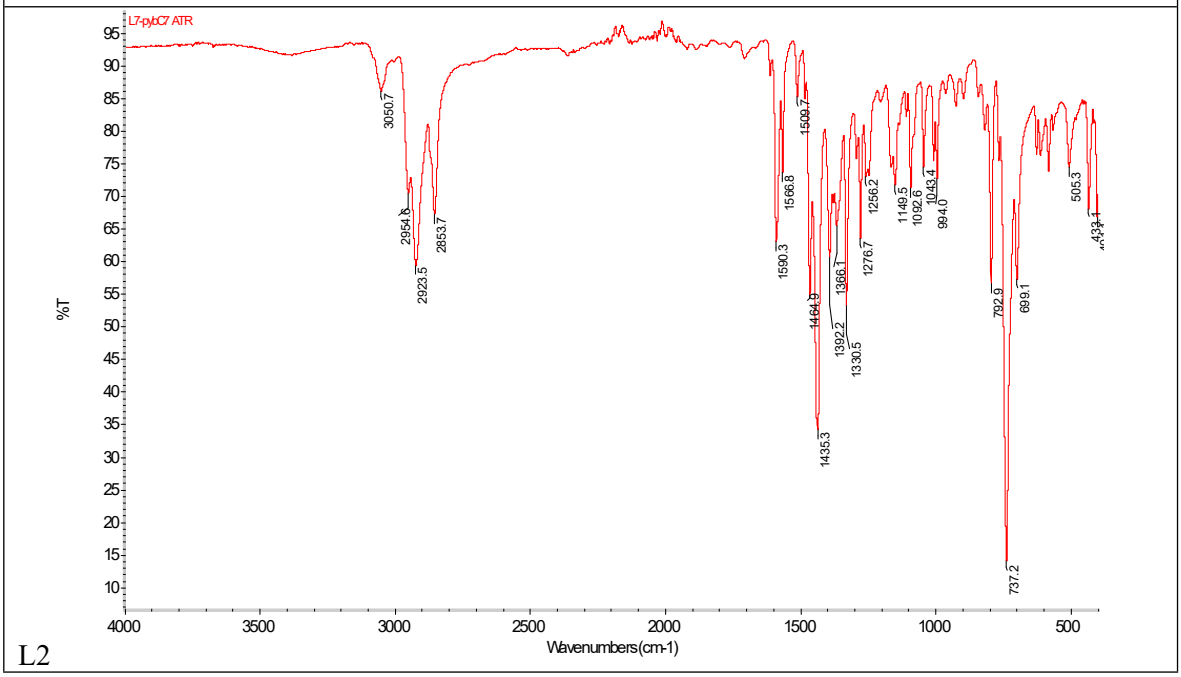
L7-pybC7 ATR
%T
Wavenumbers(cm-1)
3050.7
2954.8
2923.5
2853.7
1590.3
1566.8
1509.7
1464.9
1435.3
1392.2
1366.1
1330.5
1276.7
1256.2
1149.5
1092.6
1043.4
994.0
792.9
737.2
699.1
505.3

L2

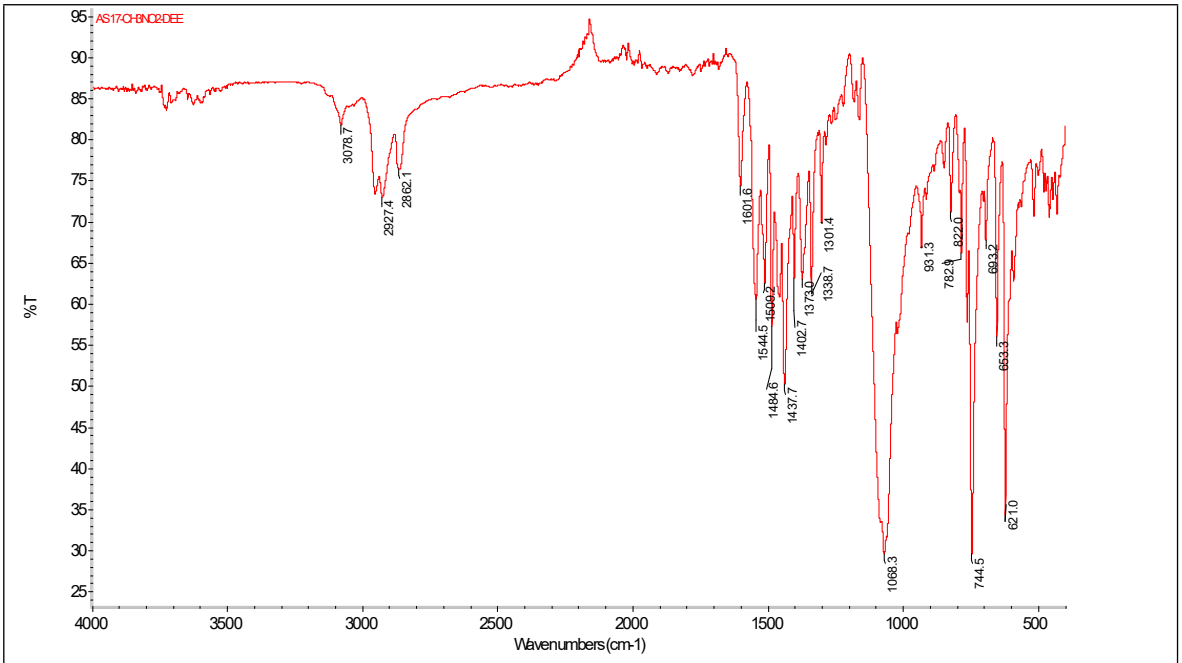

Compound **1**

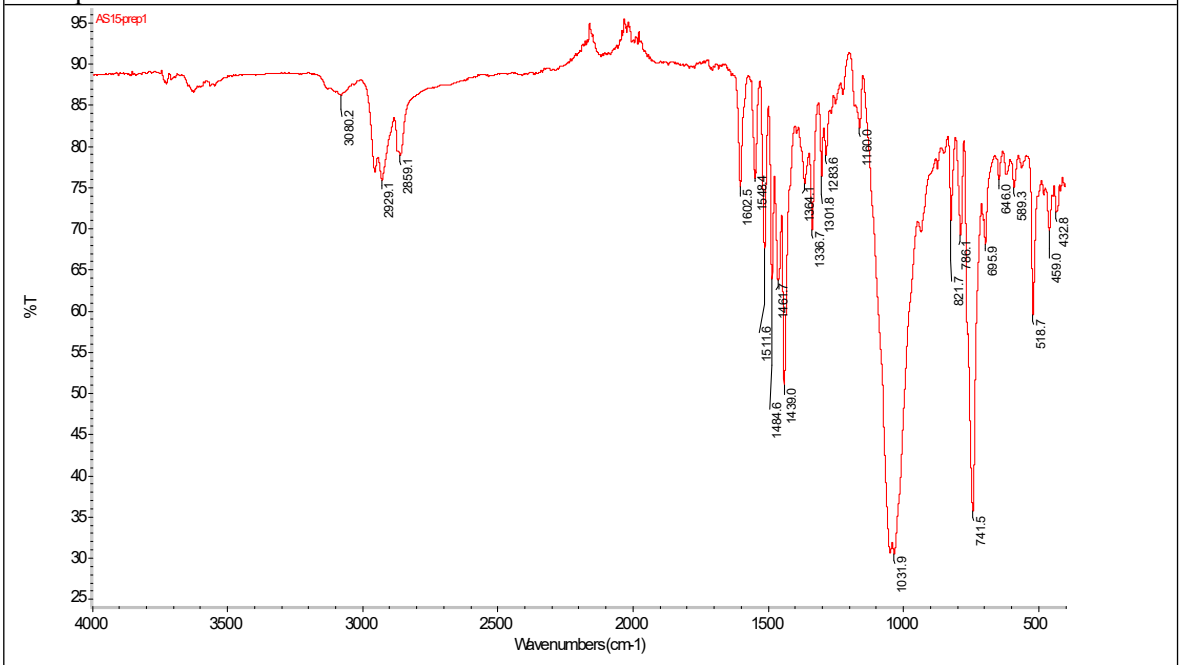

Compound **2**

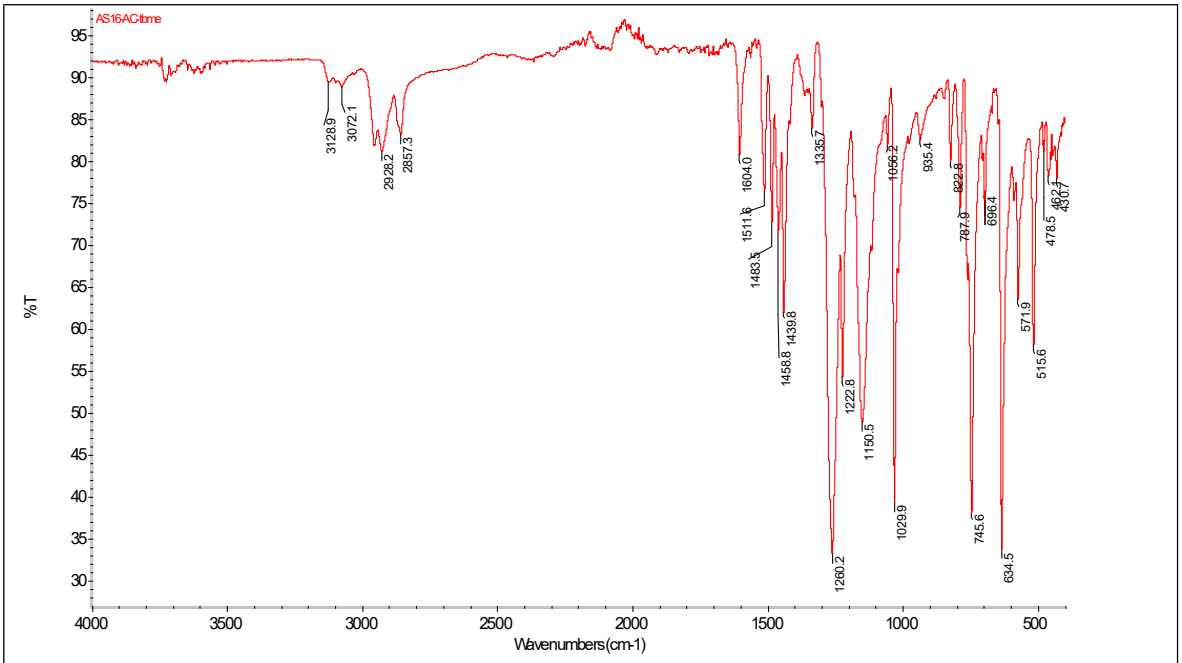

Compound **3**

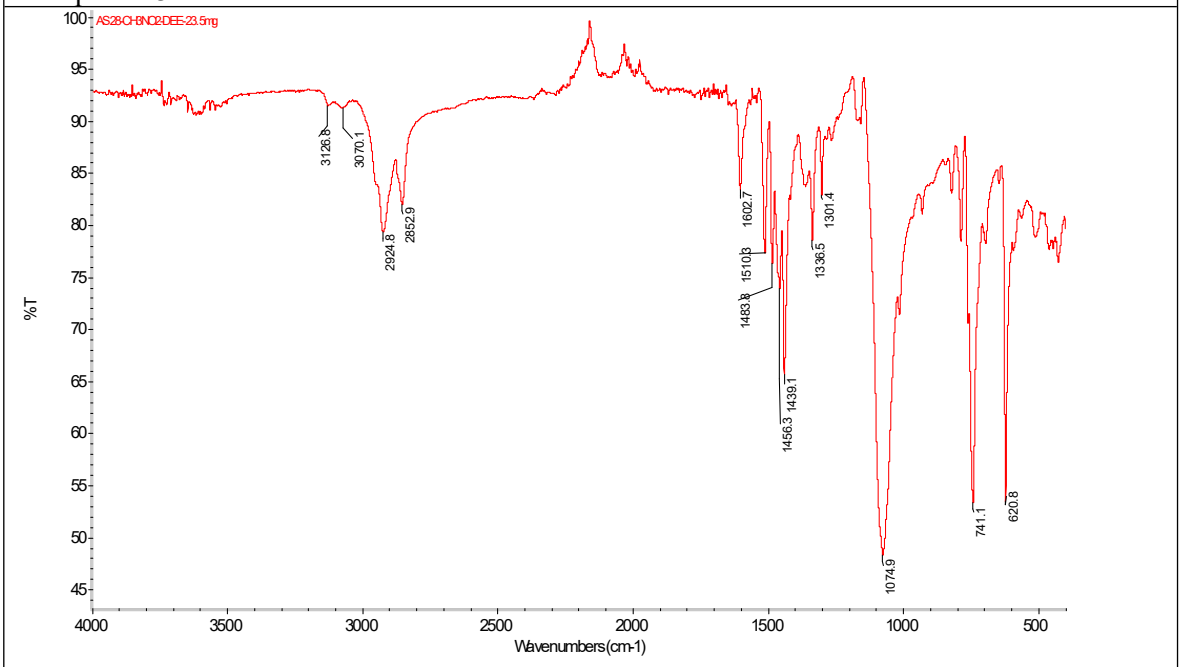

Compound **4**

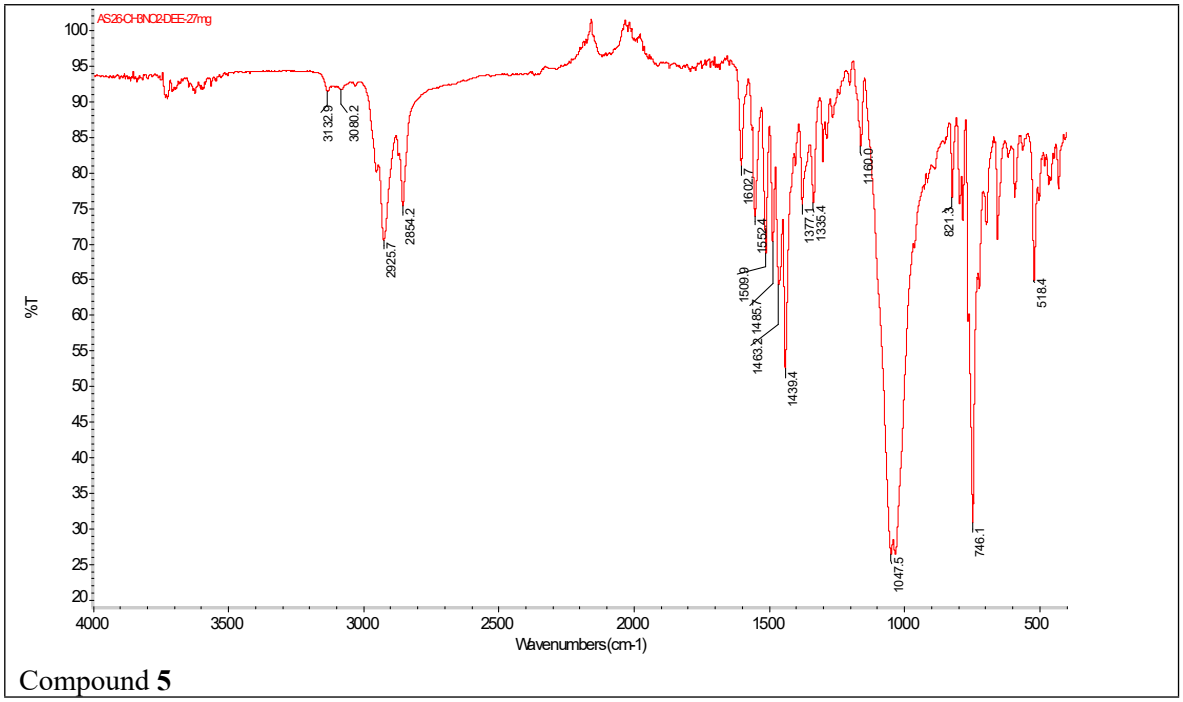

Figure S3. FTIR ATR spectra reported compounds.

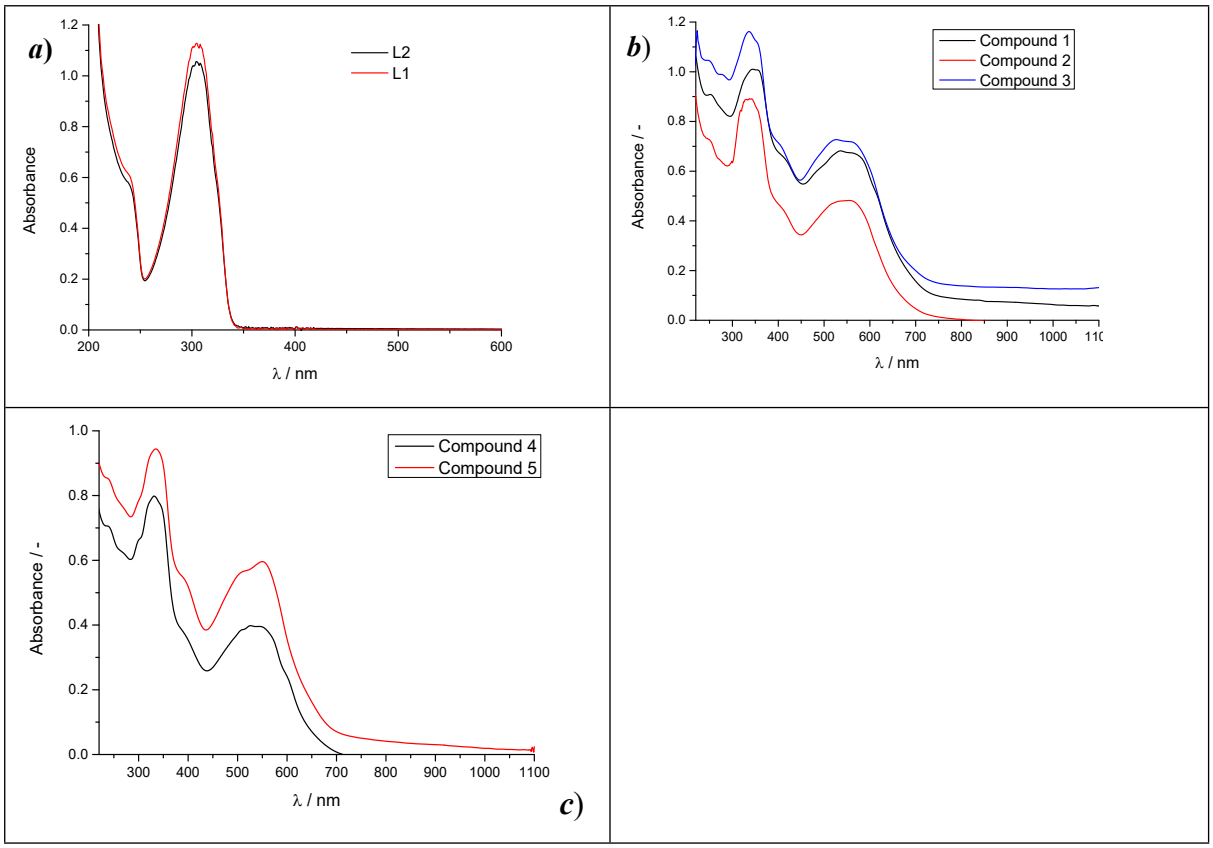

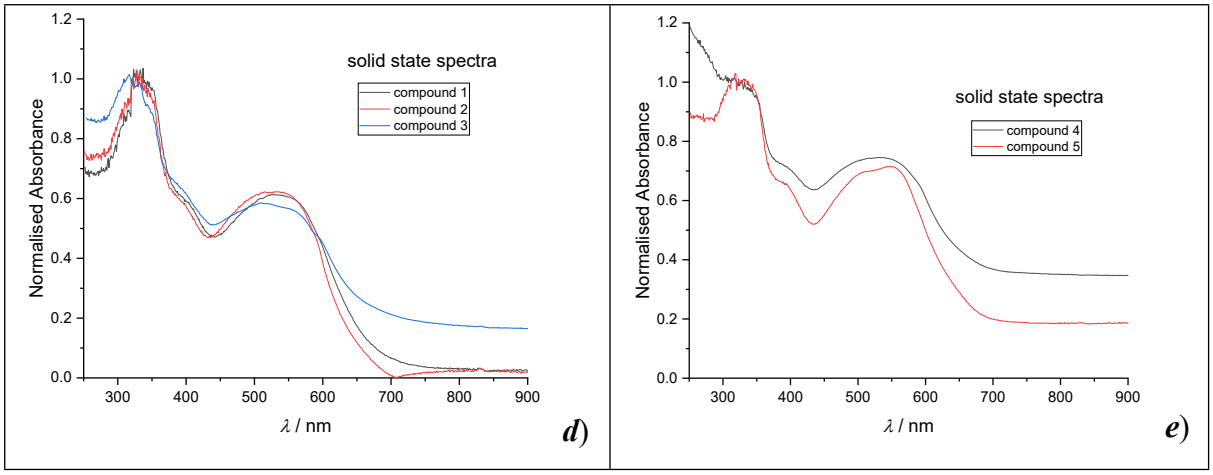

Figure S4. UV-VIS spectra of reported compounds recorded in ethanolic solution (***a***-***c***) and in the solid state (as nujol suspension ***d***, ***e***)

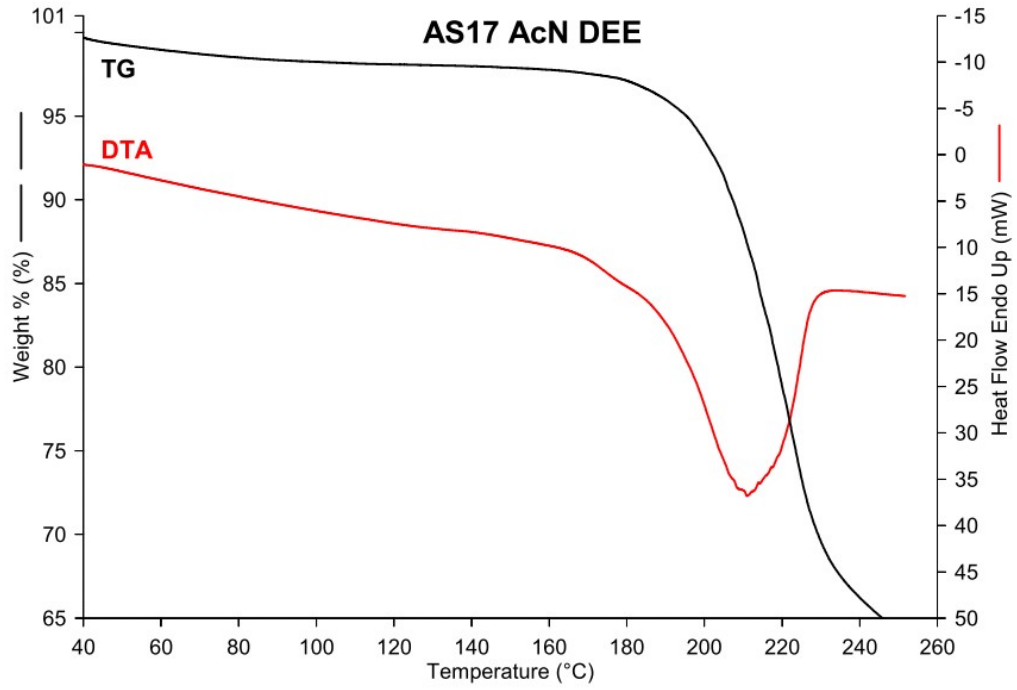

Compound **1**

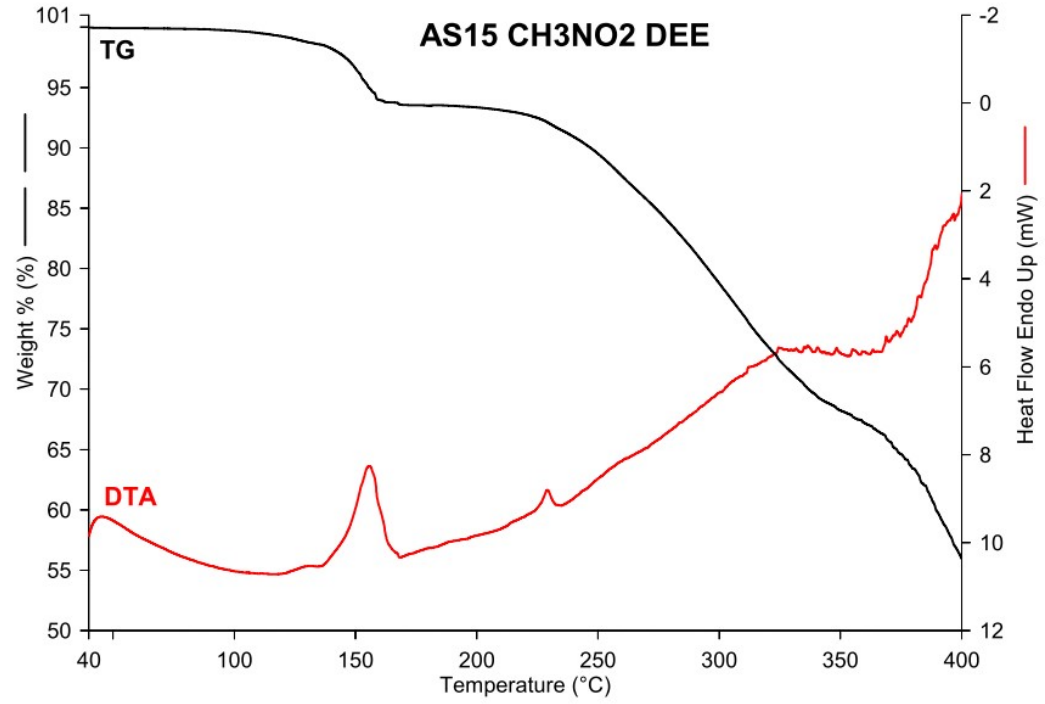

Compound **2**

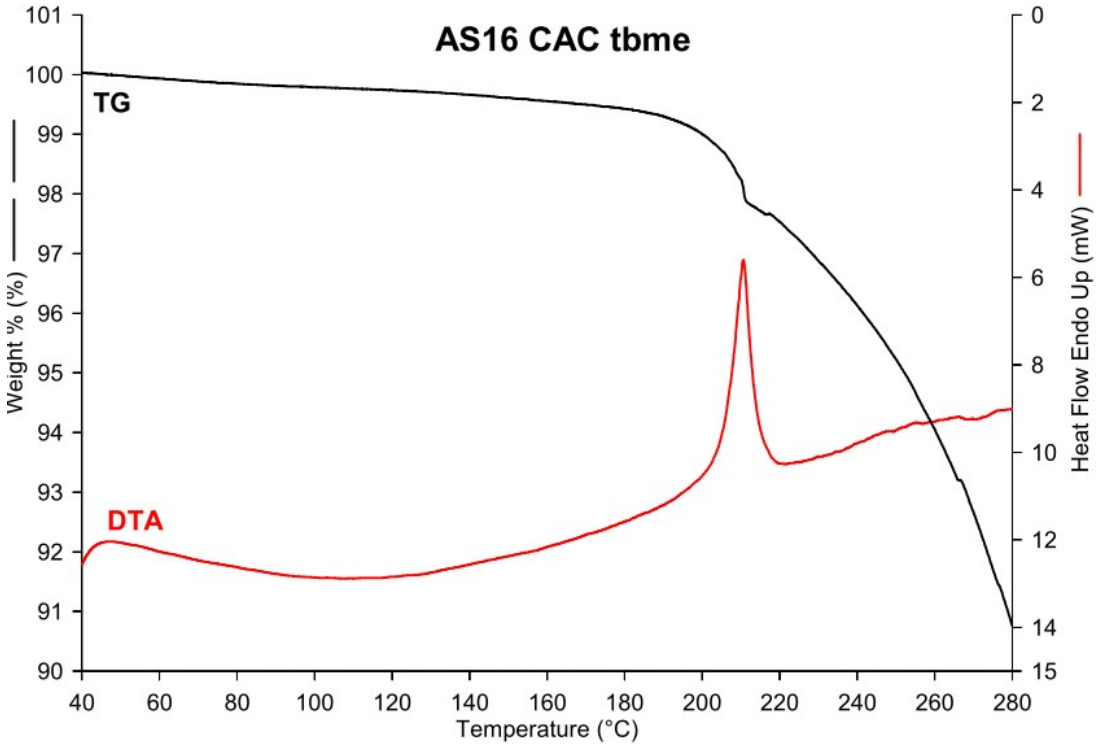

Compound **3**

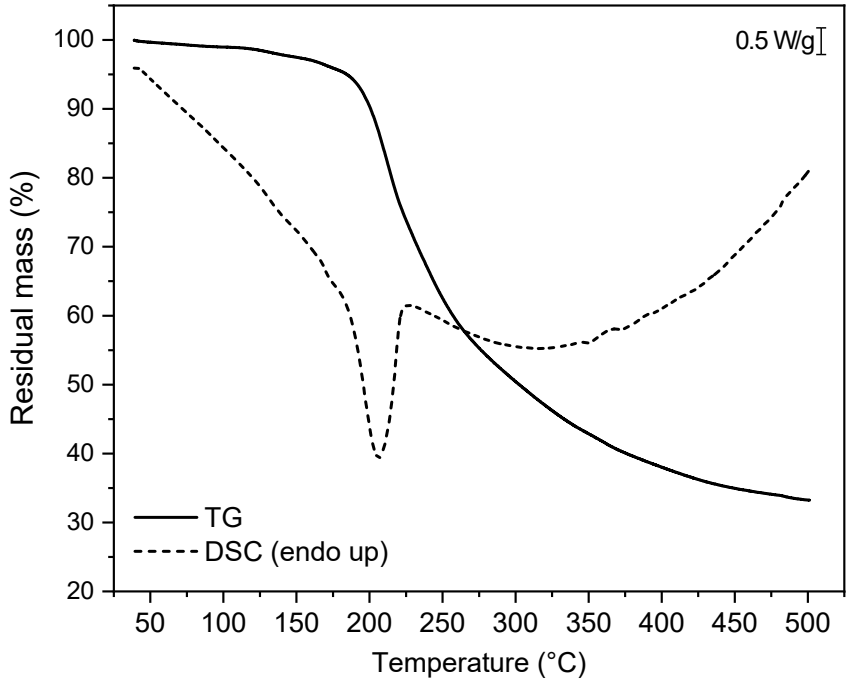

Compound **4**

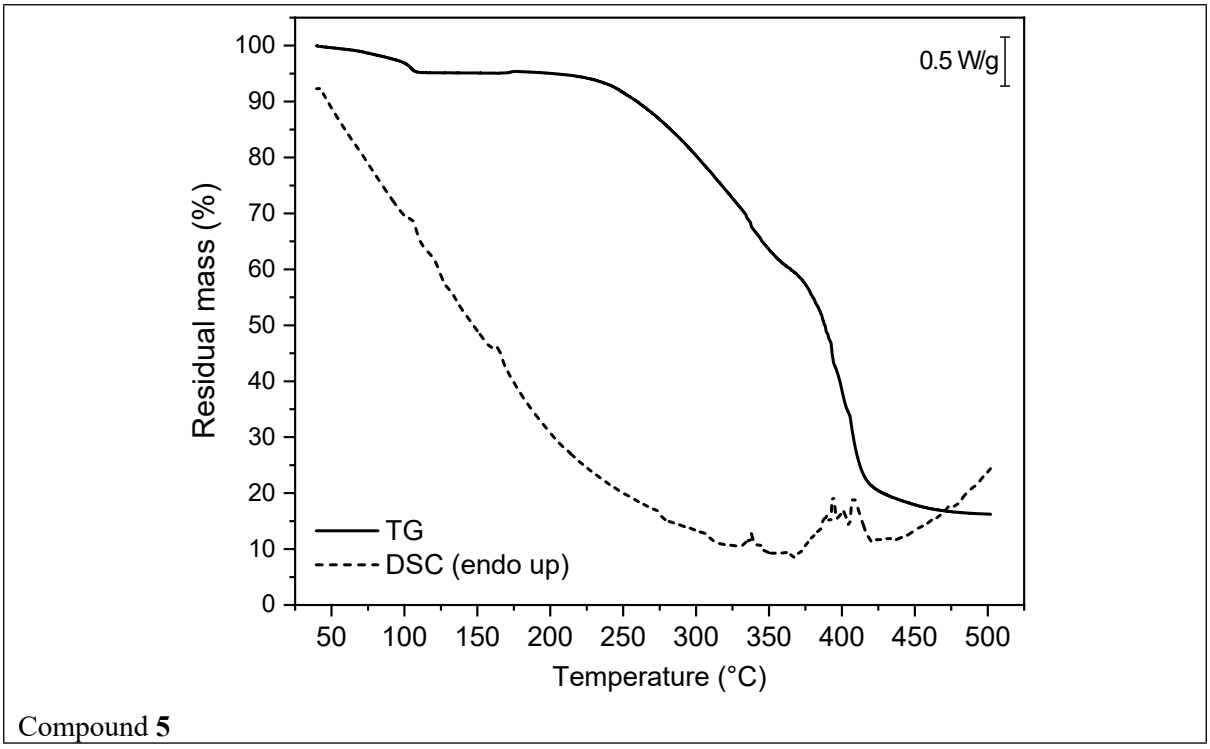

Compound **5**

Figure S5 TG/DTA and TG/DSC analyses reported compounds.

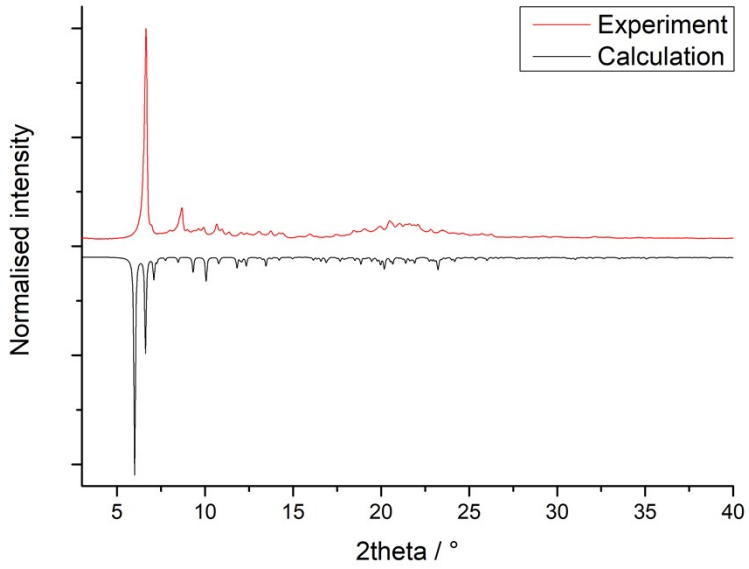

Compound **1**

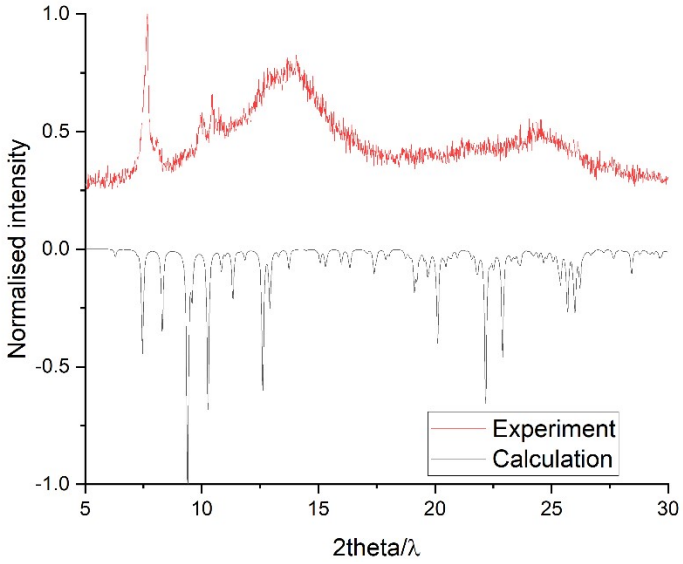

Compound **2**

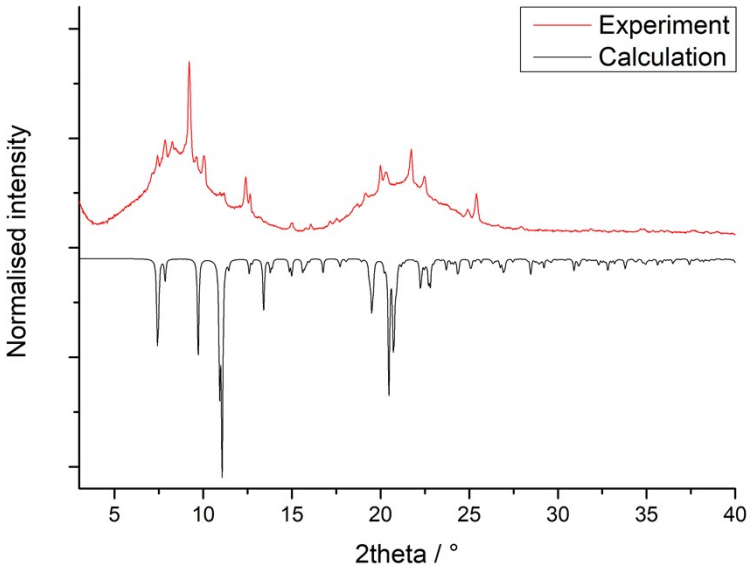

Compound **3**

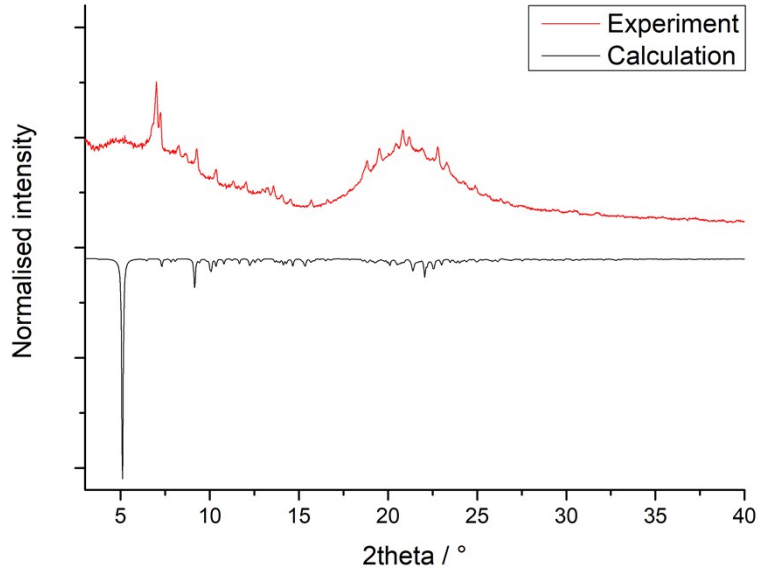

Compound **4**

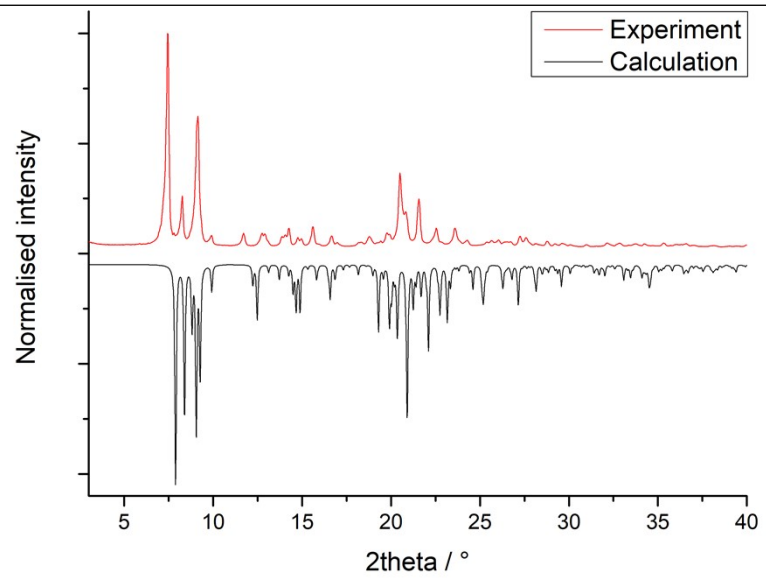

Compound **5**

Figure S6 X-ray powder diffraction patterns of reported coordination compounds

S3 Single-crystal X-ray diffraction analysis

Table S1 The structural parameters of compounds **1-5.**

	Compound **1**	Compound **2**	Compound **3**	Compound **4**	Compound **5**
Formula	$C_{53}H_{63}Fe\ N_{11}Cl_2O_{12}$	$C_{55}H_{67}B_2F_8FeN_9O$	$C_{53}H_{57}F_6FeN_9O_6S_2$	$C_{57}H_{69}Cl_2FeN_9O_8$	$C_{58}H_{72}B_2F_8FeN_{10}O_2$
Formula weight / g mol^{-1}	1172.89	1099.64	1147.42	1134.96	1170.72
Crystal colour	purple	purple	purple	purple	purple
Temperature / K	100	100	200	90	90
Wavelength / Å	1.54184	1.54184	1.54184	1.54184	1.54184
Crystal system	monoclinic	monoclinic	monoclinic	monoclinic	triclinic
Space group	*C*2/c	$P2_1/n$	*C*c	$P2_1/n$	*P*1
a / Å	29.8723(12)	17.5535(3)	15.6483(3)	14.58967(13)	10.97980(10)
b / Å	14.9781(5)	16.3130(2)	22.5038(3)	15.02560(17)	11.88790(10)
c / Å	25.2907(8)	18.8082(3)	17.2162(4)	25.1896(3)	13.16240(10)
α / °	90	90	90	90	107.3440(10)
β / °	99.778(4)	101.2251(17)	116.119(3)	96.9658(10)	110.6770(10)
γ / °	90	90	90	90	103.1580(10)
V / Å^3	11151.4(7)	5282.7(16)	5443.5(2)	5481.28(10)	1423.71(2)
Z; ρ_{calc} / g.cm^{-3}	8; 1.131	4; 1.383	4; 1.403	1; 1.375	1; 1.365
μ (Cu-Kα)/mm^{-1}	3.647	2.947	3.609	3.622	2.786
F(000)	4912.0	2304.0	2392.0	2392	614.0
Final R indices [I > 2σ(I)][a]	R_1 = 0.1035, wR_2 = 0.2905	R_1 = 0.0570, wR_2 = 0.1409	R_1 = 0.0510, wR_2 = 0.1368	R_1 = 0.0374, wR_2 = 0.0913	R_1 = 0.0430, wR_2 = 0.1145
R indices (all data)[a]	R_1 = 0.1339, wR_2 = 0.3150	R_1 = 0.0626, wR_2 = 0.1445	R_1 = 0.0550, wR_2 = 0.1401	R_1 = 0.0416, wR_2 = 0.0934	R_1 = 0.0449, wR_2 = 0.1159
GoF on F^2	1.079	1.056	1.015	1.025	1.062
CCDC deposit number	2352248	2352249	2352250	2352251	2352252

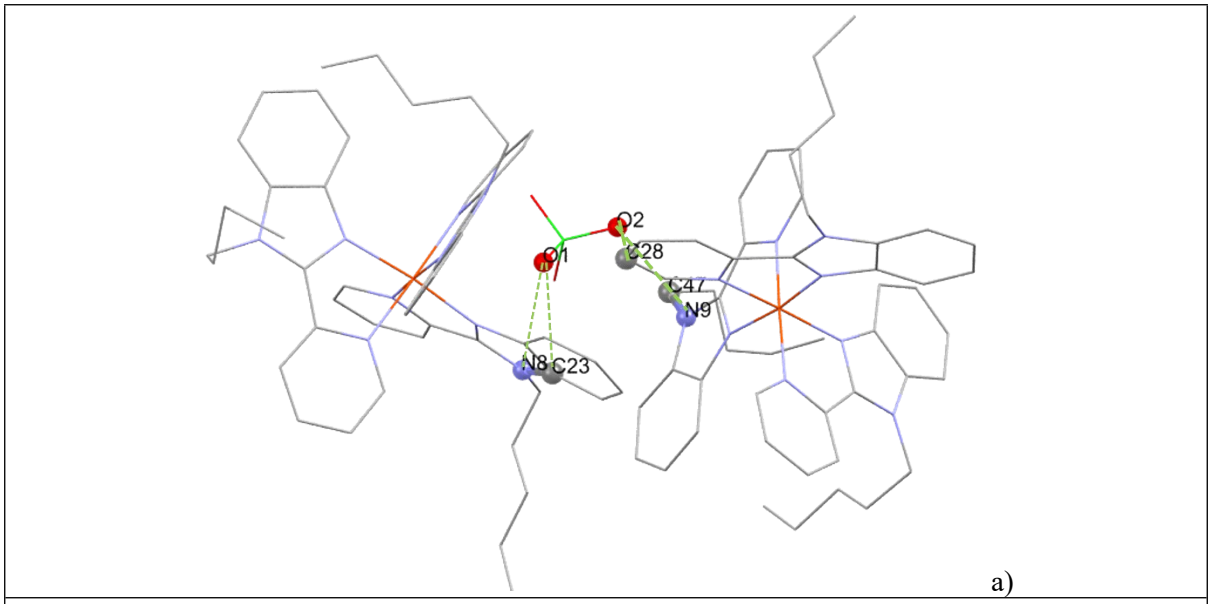
O2
O1
C28
C47
N9
N8
C23

a)

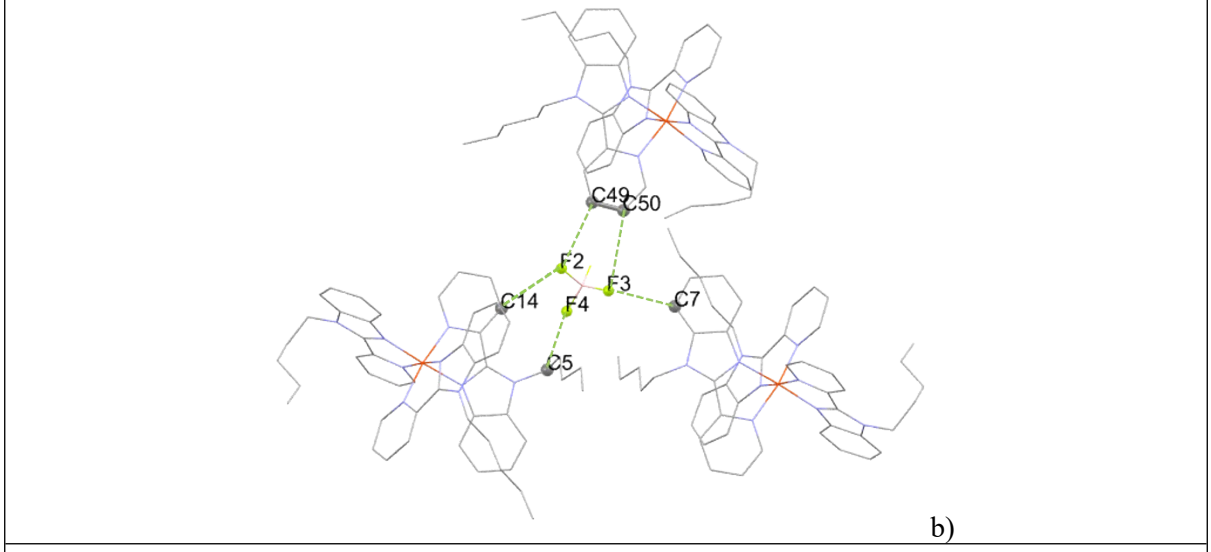
C49
C50
F2
F3
C14
F4
C7
C5

b)

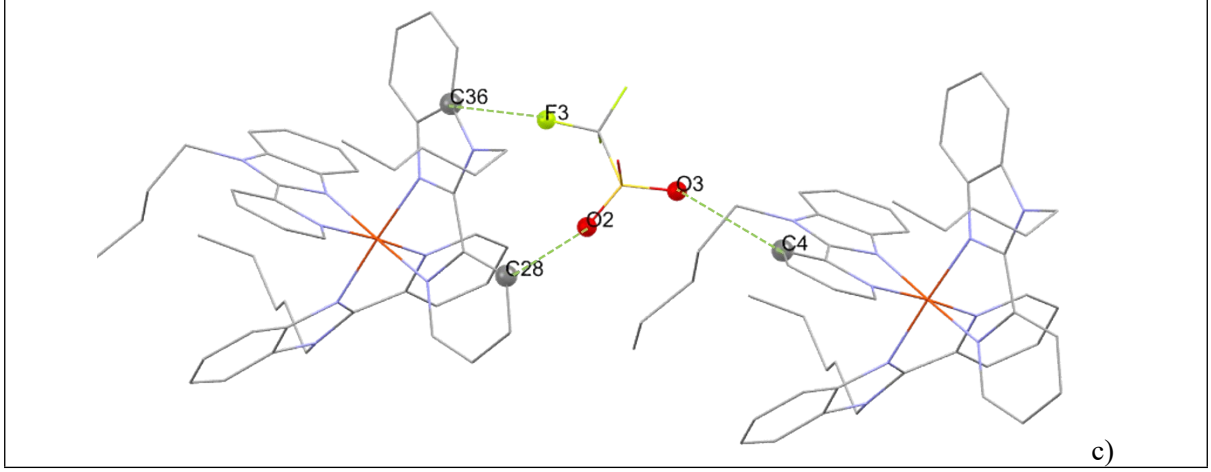
C36
F3
O3
O2
C4
C28

c)

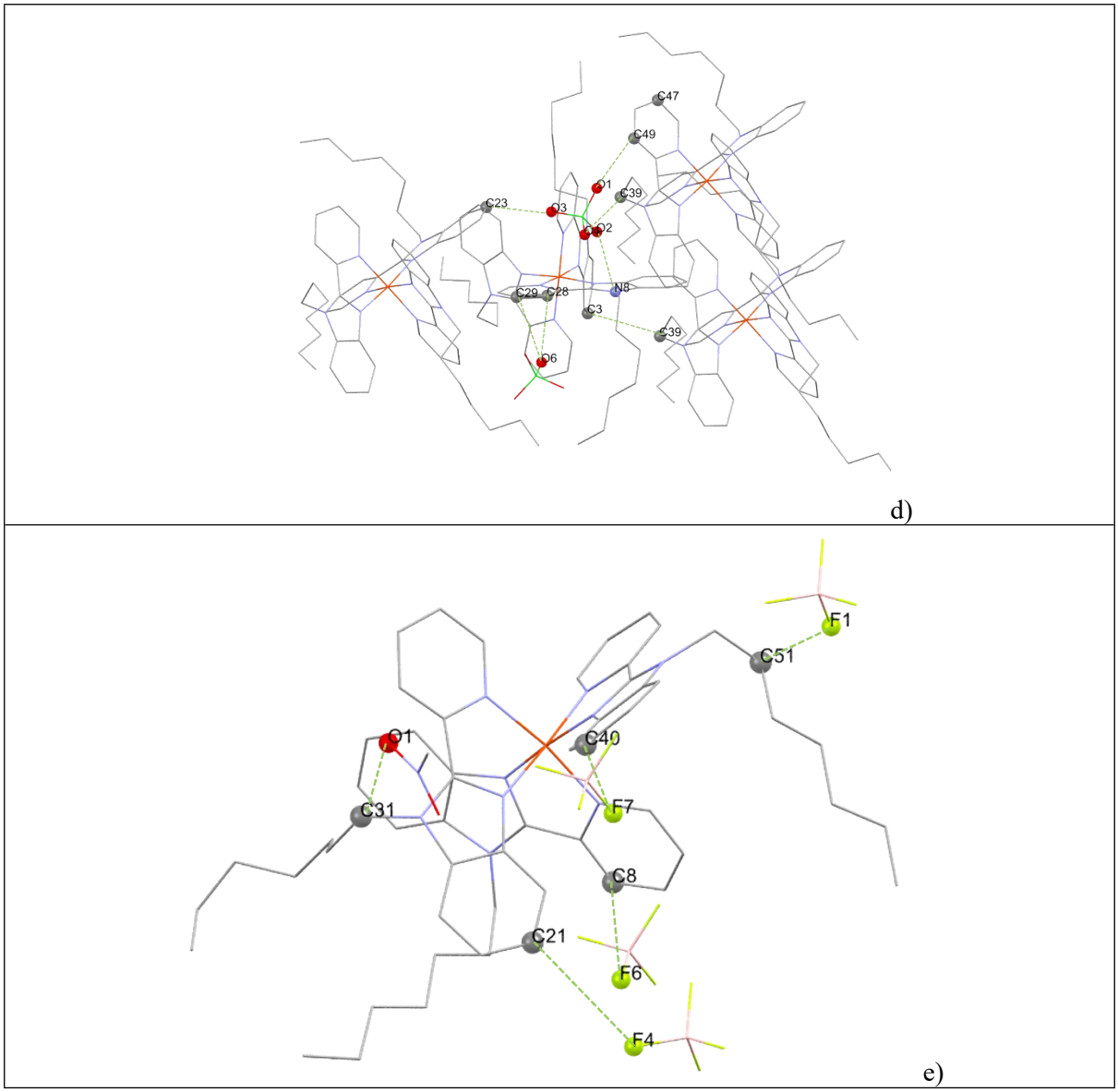

Figure S7 Visualisation of intermolecular non-covalent contacts in the reported compounds: ***a***)

1: ***a***) C28···C23=3.345(7) Å; O2···N9=3.07(1) Å; O1···N8=3.114(7) Å; O2···C47=3.30(1) Å; ***b***) **2**: F2···C14=3.154(4) Å; F2···C49=3.213(4) Å; F3···C7=3.085(4) Å; F3···C50=3.541(5) Å; F4···C5=3.437(6) Å;F4···C14=3.443(5) Å; ***c***) **3**: F3···C36=3.098(8) Å; O2···C28=3.17(2) Å; O3···C4=2.99(1) Å; ***d***) **4**: O6···C29=3.175(2) Å; O6···C28=3.072(2) Å; C39···C3=3.390(3) Å; O2···N8=2.920(2) Å; O3···C23=3.140(3) Å; O1···C49=3.073(2) Å; C39···O4=3.124(2) Å; ***e***) **5**: F7···C40=3.472(7) Å; F6···C8=3.216(5) Å; F4···C21=3.568(5) Å; F1···C51=3.134(7) Å; O1···C31=3.181(8) Å;

Table S2 Bond distances and structural parameters of coordination polyhedra of reported compounds

	1 @ 100 K	**2** @ 100 K	**3** @ 200 K	**4** @ 150 K	**5** @ 90 K
	Fe1	**Fe1**	**Fe1**	**Fe1**	**Fe1**
Fe-N1 / Å	1.990(5)	1.990(2)	1.975(4)	1.9913(15)	1.979(3)
Fe-N2 / Å	2.006(5)	1.978(2)	1.969(4)	1.9735(15)	1.988(3)
Fe-N3 / Å	1.962(5)	1.978(2)	1.983(5)	1.9582(16)	1.976(4)
Fe-N4 / Å	1.995(5)	1.967(2)	1.966(5)	1.9820(16)	1.973(3)
Fe-N5 / Å	1.971(5)	1.955(2)	1.974(5)	1.9690(15)	1.962(3)
Fe-N6 / Å	1.982(5)	1.993(2)	1.987(5)	1.9720(15)	1.988(3)
Σ / º	66.0	66.1	71.3	68.5	65.8
Θ / º	128.2	135.4	117.8	120.9	124.1
HP-6[a]	27.1	28.2	26.6	26.9	27.3
PPY-6[a]	26.8	27.1	26.9	26.7	27.6
OC-6[a]	**0.8**	**0.8**	**0.7**	**0.7**	**0.7**
TPR-6[a]	14.6	14.6	15.5	14.6	15.3
JPPY-6[a]	29.9	30.6	29.9	29.9	30.7

[a]Results of the SHAPE calculations for coordination polyhedra of hexagon (HP-6), pentagonal pyramid (PPY-6), octahedron (OC-6), trigonal prism (TPR-6), Johnson pentagonal pyramid (JPPY-6).

1

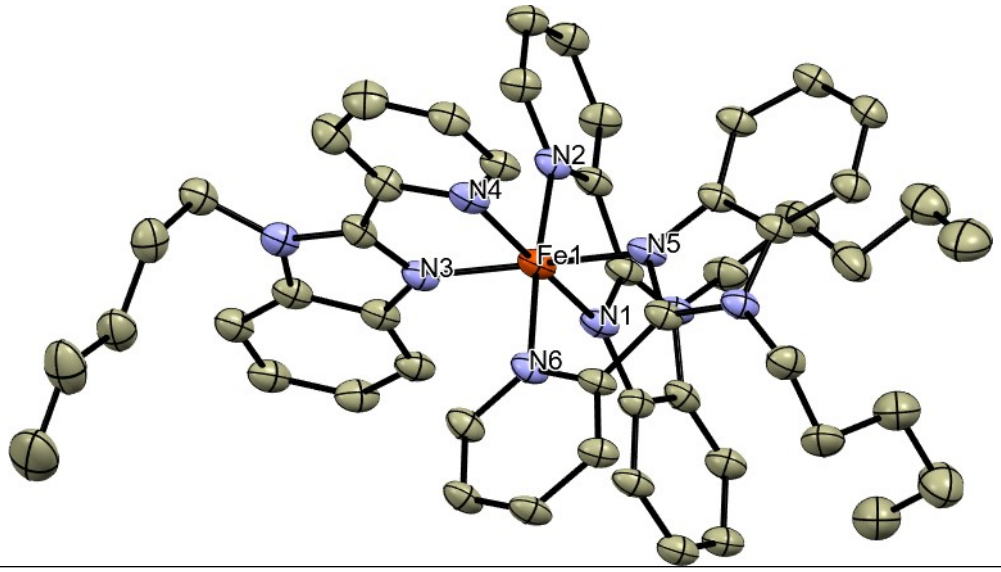

2

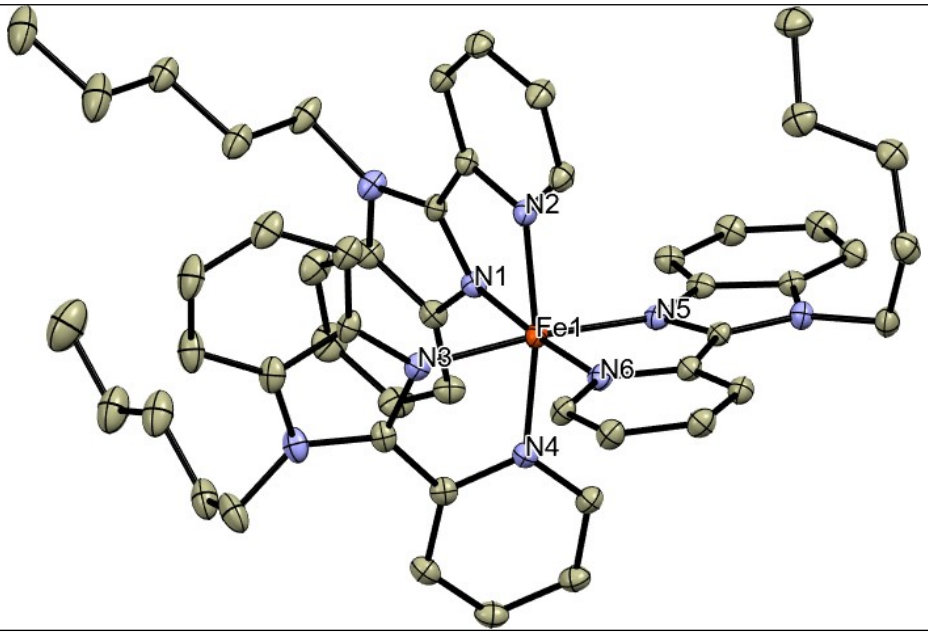

3

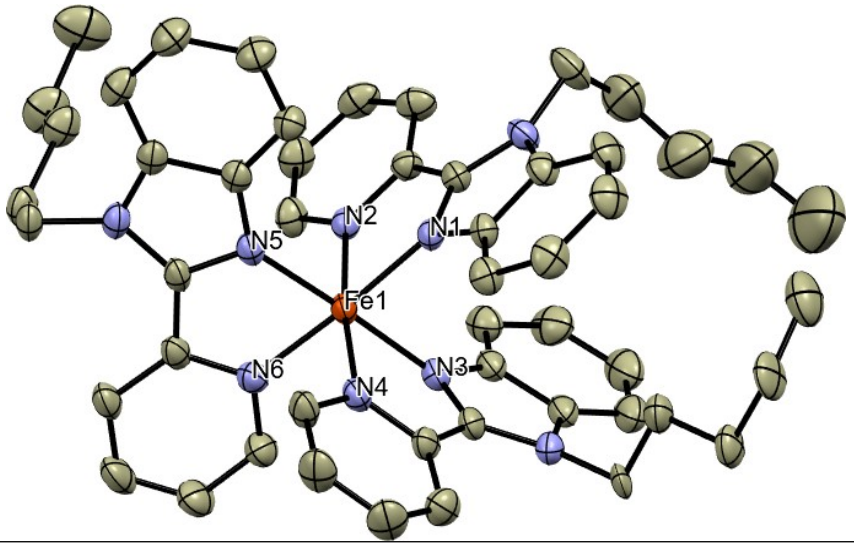

4

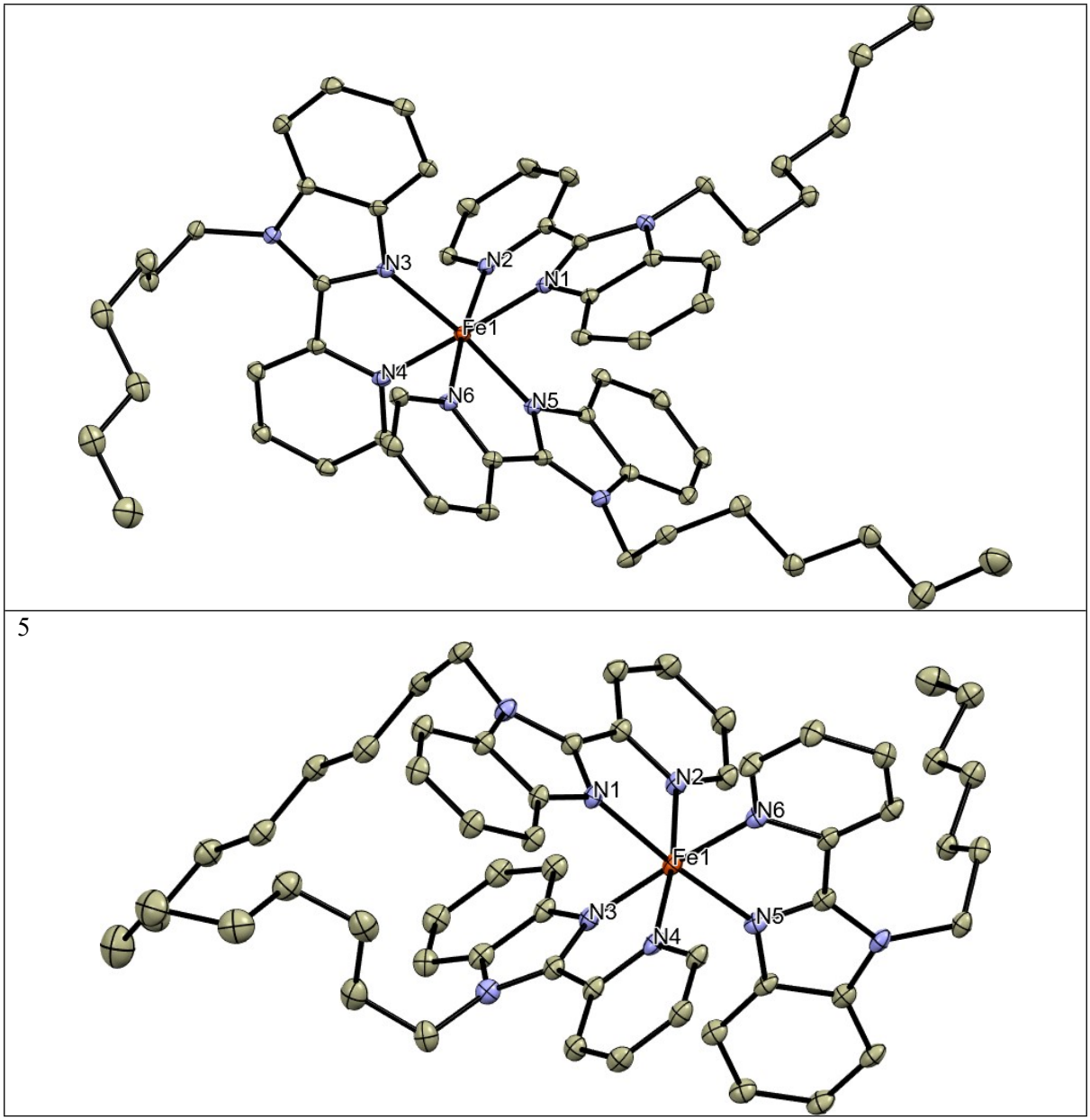

Fig. S8 ORTEP representations of the complex molecules in **1-5** with atomic displacement parameters set to a 30% probability level. Hydrogen atoms, anions, solvent molecules, and disordered parts with minor occupancy were omitted for clarity.

S4 Magnetic properties and computational studies

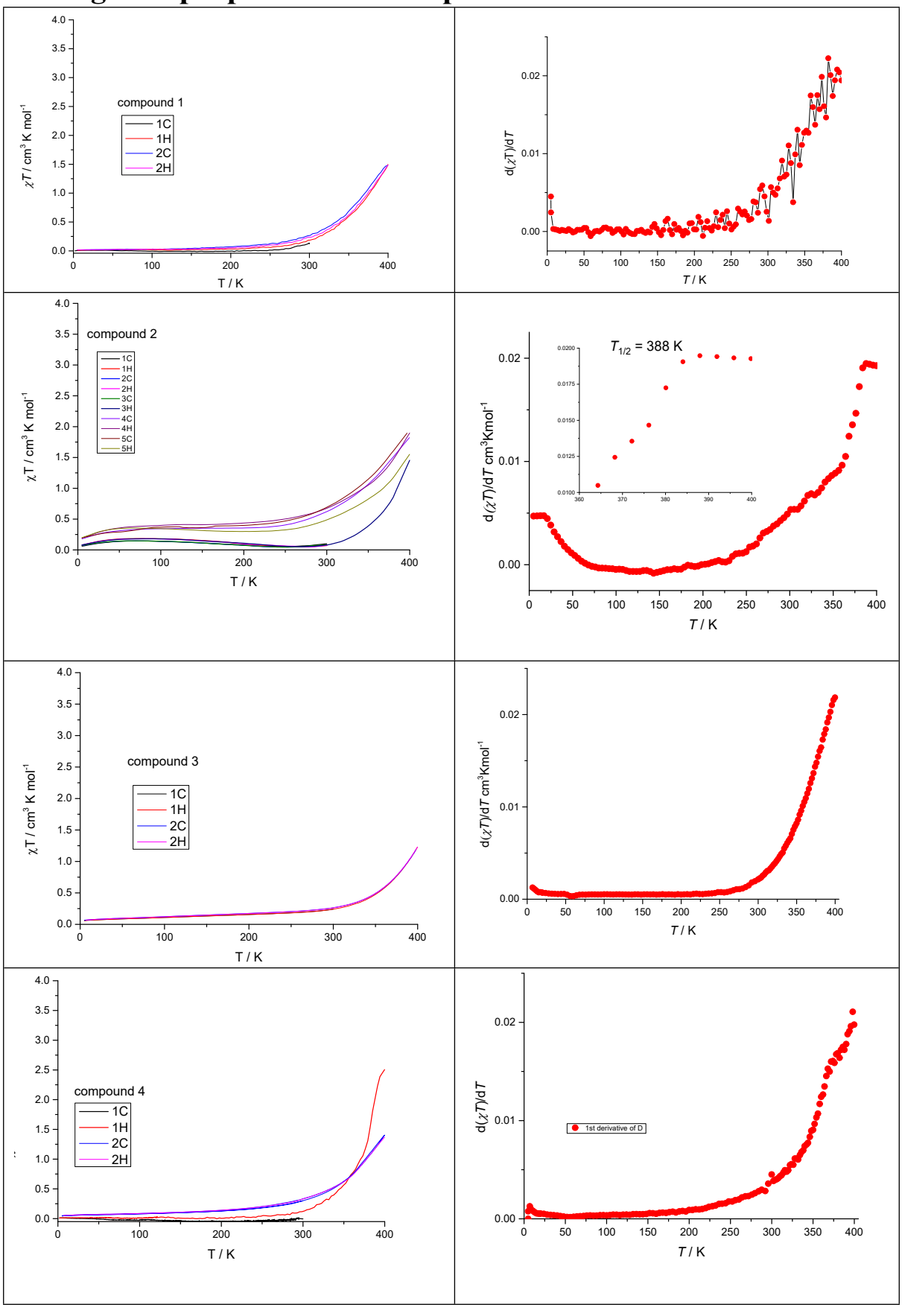

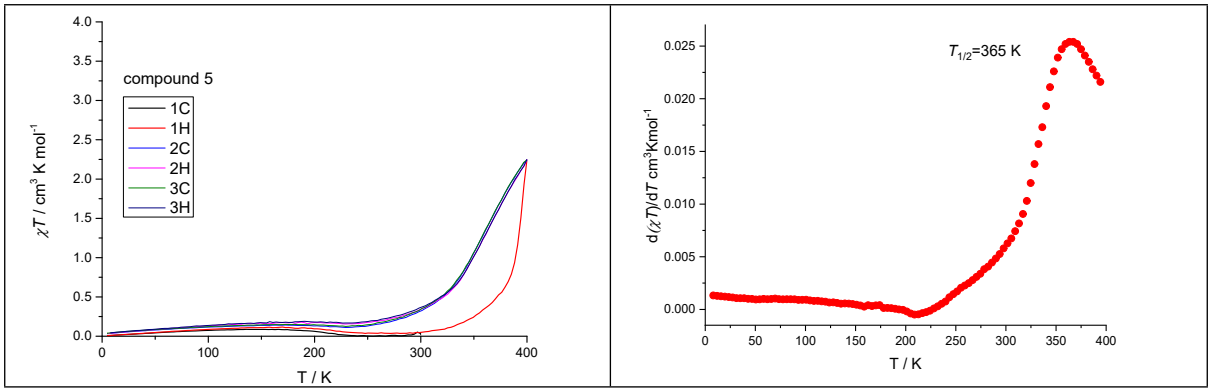

Figure S9 ***a***) Temperature variable magnetic properties of reported compounds recorded in several heating(H)/cooling(C) cycles; ***b***) first derivative o χT vs T curves for reported compounds each determined from the last heating curves.

S5 Surface characterization techniques

To investigate the crystalline order within the deposited molecular films, grazing-incidence wide-angle X-ray scattering (GIWAXS) measurements were performed using a compact laboratory X-ray scattering system (Nanostar, Bruker). As shown in Figure S10, the GIWAXS pattern of the self-assembled SCO layer exhibits two side maxima. This observation suggests the presence of a uniaxial texture within the molecular film. While a limited number of weak diffractions prevented a definitive determination of the precise molecular axis orientation relative to the substrate surface, the presence of in-plane diffractions at $q \approx 1.5$ Å^{-1} provides clear evidence for crystalline order within the deposited film.

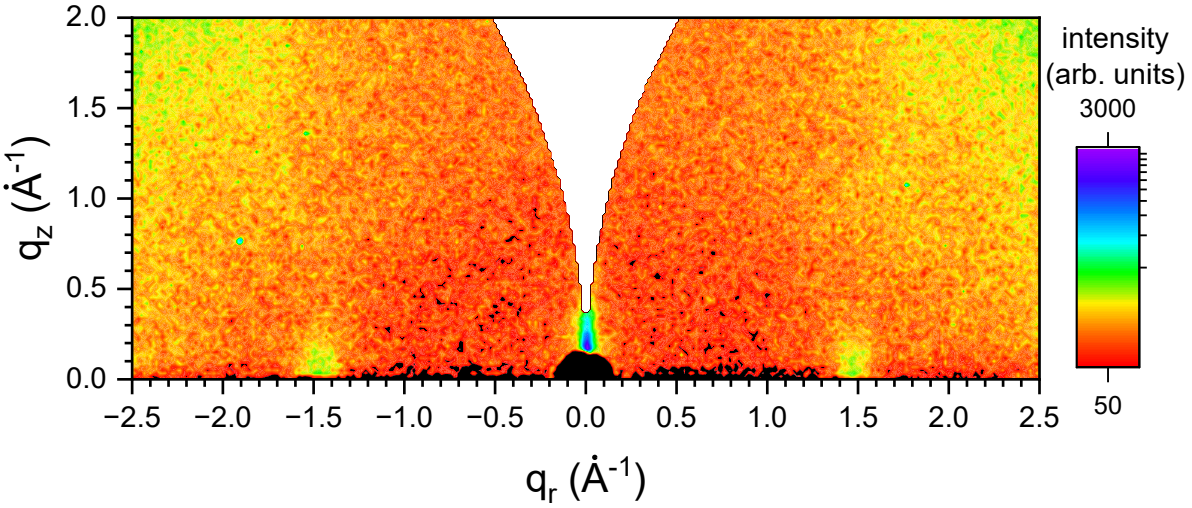

Figure S10 GIWAXS pattern of self-assembled SCO on Si substrate.

The AFM images of self-assembled molecular films were acquired in tapping mode with Dimension Edge AFM (Veeco) using RTESPA-300 etched silicon tips. The optical profilometer Contour (Bruker) was employed to map the film homogeneity by a 5x objective using phase-shifting interferometry mode. The film thickness was estimated by spectroscopic ellipsometry in the spectral range 240 – 800 nm using SE 800E ellipsometer (Sentech).

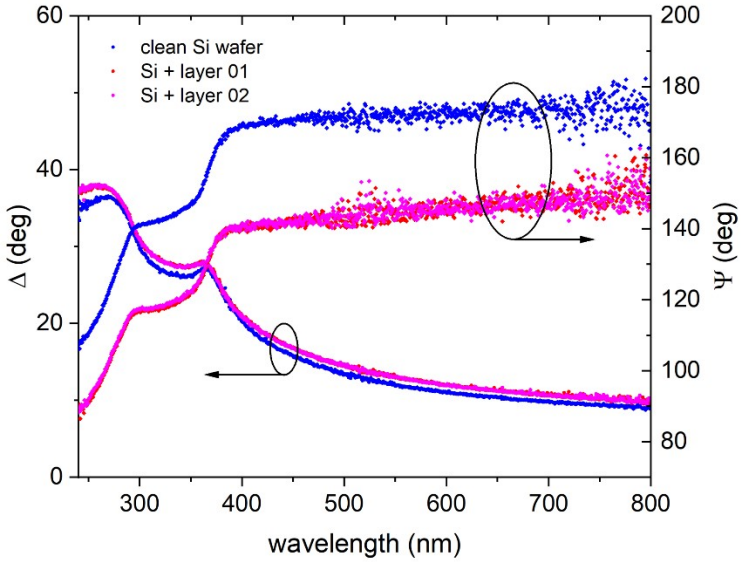

Figure S11 Measured (Δ_e, Ψ) parameters of clean Si and Si with self-assembled SCO layers. Layers 1 and 2 refer to two different samples used to validate the reproducibility of SCO layer deposition.

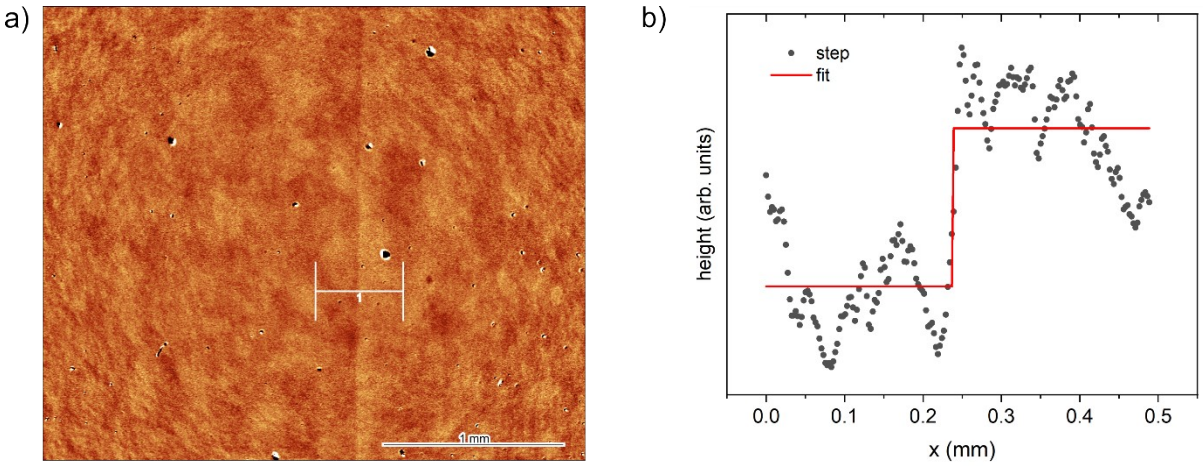

Figure S12 Height profile of a self-assembled SCO film on a Si substrate. a) Phase-shifting interferometry (PSI) image documents the surface profile of the sample. PSI cannot provide the exact number of layer thicknesses for optically transparent thin films but helps assess the spatial homogeneity of the film. SCO molecular film was etched by O_2 plasma on a part of the sample. b) The height along the line profile 1 indicates the step between the pristine and etched areas.

---

[1] C. G.Wahlgren and A. W. J. Addison, Heterocycl. Chem., 1989, **26**, 541–543.
[2] Rigaku Oxford Diffraction (2020) CrysAlisPro 1.171.40.82a.
[3] G. M. Sheldrick, *Acta Crystallogr. Sect.* 2015, ***A*** **71**, 3–8.
[4] L. J. Bourhis, O. V. Dolomanov, R. J. Gildea, J. A. K. Howard and H. Puschmann, *Acta Crystallogr. Sect. A 71* 2015, 59–75.
[5] O. V. Dolomanov, L. J. Bourhis, R. J. Gildea, J. A. K. Howard and H. Puschmann, *J. Appl. Crystallogr.*, 2009, **42**, 339–341.
[6] P. van der Sluis and A. L. Spek, Acta Cryst, 1990, **A46**, 194-201,
[77] R. Boča, Theoretical Foundations of Molecular Magnetism, Elsevier, Amsterdam, 1999
[8] a) F. Neese, Software Update: The ORCA Program System—Version 5.0. *WIREs Comput. Mol. Sci.* 2022; b) F. Neese, The ORCA Program System. *WIREs Comput. Mol. Sci.* 2012, **2**, 73–78..
[9] A. D. Becke, *Phys. Rev. A*, 1988, **38**, 3098–3100.
[10] a) F. Weigend, *Phys. Chem. Chem. Phys.* 2002, **4**, 4285–4291; b) F. Weigend and R. Ahlrichs, *Phys. Chem. Chem. Phys.* **2005**, 7, 3297–3305.
[11] Y. Guo, K. Sivalingam, E. F.Valeev and F. Neese. *J. Chem. Phys.* 2017, **147**, 064110.
[12] a) L. Lang, M. Atanasov and F. Neese, *J. Phys. Chem. A*, 2020, **124**, 1025–1037; b) M. Atanasov, D.

Ganyushin, K. Sivalingam, F. Neese, In *Structure and Bonding*; 2011; pp 149–220..
[13] a) F. Neese, F. Wennmohs, A. Hansen and U. Becker, *Chem. Phys.* 2009, **356**, 98–109; b) A. K. Dutta, F. Neese and R. Izsák, *Mol. Phys.* 2018, **116**, 1428–1434. c) R. Izsák and F. Neese, *J. Chem. Phys.* 2011, **135**, 144105.
[14] M. D. Hanwell, D. E.Curtis, D. C. Lonie, T. Vandermeersch, E. Zurek and G. R. Hutchison, *J. Cheminform.* 2012, **4**, 17.
[15] C. F. Macrae, P. R. Edgington, P. McCabe, E. Pidcock, G. P. Shields, R. Taylor, M.Towler and J.van de Streek, *J. Appl. Crystallogr.* 2006, **39**, 453–457.
[16] Jon Kragskow and Nicholas Chilton 2022. *Magnetism Tools, Tanabe Sugano.* Accessed 4. 10. 2023. https://magnetism-tools.manchester.ac.uk/apps/tanabe_sugano_app.
[17] OpenAI. (2023). *ChatGPT* (4. 10. 2023, version 3.5.) [Large language model]. https://chat.openai.com